

CHAPTER IV

RESULTS AND DISCUSSION

Photocatalytic degradation can be applied to remove many organic compounds from wastewater. In this study, titania and zinc oxide were used as photocatalyst to eliminate diuron from water. The photocatalysts were prepared by sol-gel method. Physical properties of the synthesized photocatalysts were investigated by many techniques. Then, they were compared in the photocatalytic degradation of diuron.

4.1 Properties of Synthesized Photocatalysts

4.1.1 Synthesized zinc oxide

In this research, zinc oxide was synthesized by sol-gel method and subsequently calcined at 500°C for 2 hours. Ammonia was also added during sol-gel process. The content of ammonia investigated was 0%, 7% and 28% by mass, respectively. Characterization techniques such as XRD, SEM, BET and TGA were used to investigate physical properties of the synthesized zinc oxide.

Phase composition of the zinc oxide powder was identified through XRD. XRD patterns of the zinc oxide synthesized in all conditions are shown in Figure 4.1. All of the diffraction peaks could be indexed as zinc oxide in wurzite structure. The crystallite sizes of zinc oxide calculated from the Scherer equation are shown in Table 4.1. No diffraction peaks corresponding to other phases are detected, even when high content of ammonia was added to the gel.

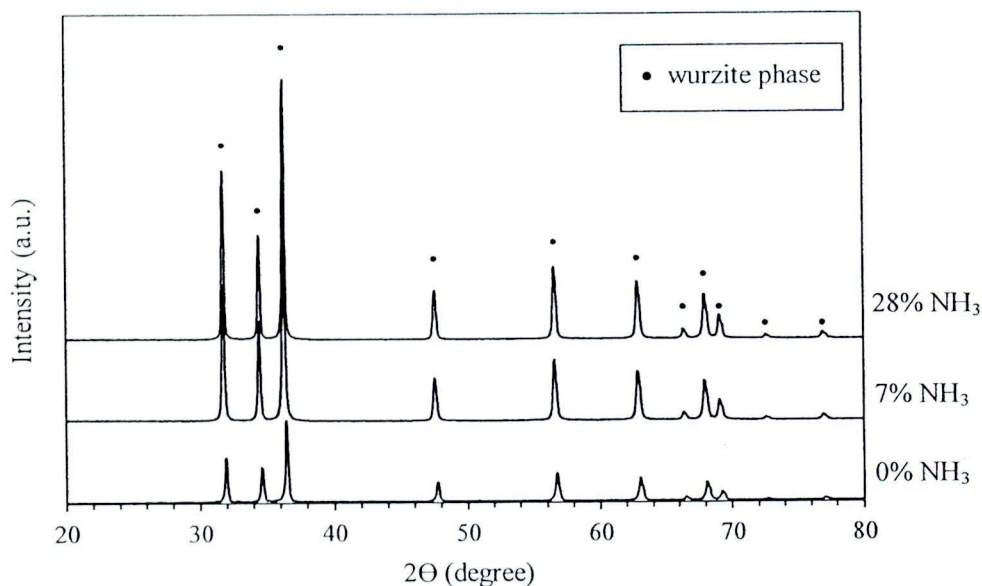


Figure 4.1 XRD patterns of the zinc oxide powder synthesized with the addition of ammonia in the amount of 0%, 7%, and 28% by weight of the solution. All products were calcined at 500°C for 2 hours.

Table 4.1 Crystallite size and surface area of the synthesized zinc oxide.

Condition of ammonia added in the solution	Crystallite size, (nm)	Specific surface area, S_{BET} , (m^2/g)	Average pore diameter (nm)	Band gap (eV)
0%	104	4	5	3.16
7%	106	8	11	3.14
28%	116	6	11	3.12

The specific surface areas of zinc oxide measured by nitrogen adsorption (S_{BET}) are also shown in Table 4.1. All samples showed Type - II adsorption/desorption isotherm which indicated the non – porous in the catalyst as shown in Figure 4.2. As the mass fraction of ammonia was increased from 0% to 7%, the specific surface area of the ZnO powder increased from 4 to 8 m^2/g while the further increase of ammonia content 28% the resulted in the decrease surface area to 6 m^2/g . However, the specific surface areas of zinc oxide are similar, so that the ammonia content did not affect to the specific surface area of zinc oxide.

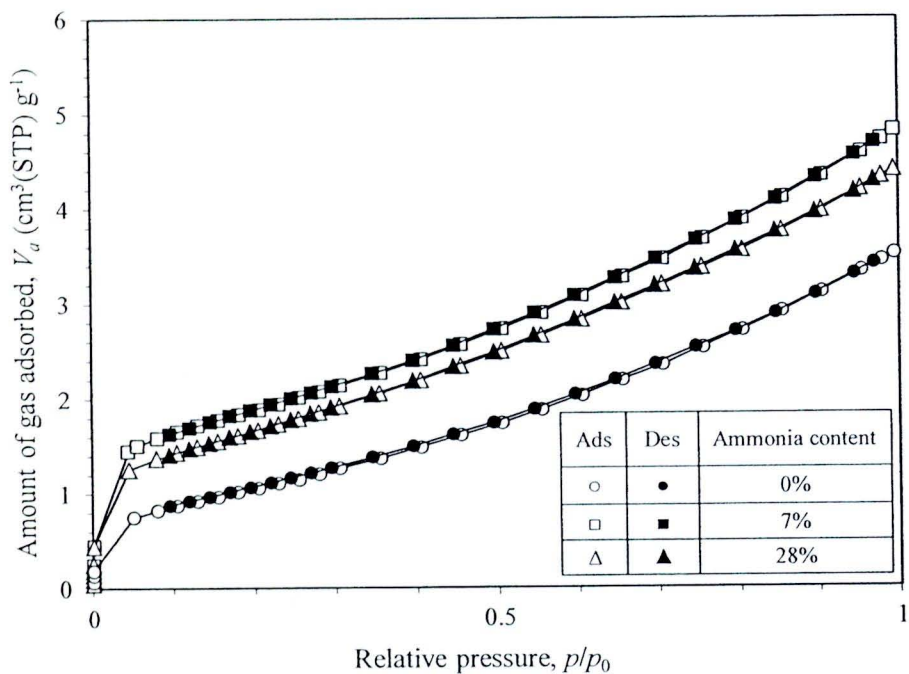
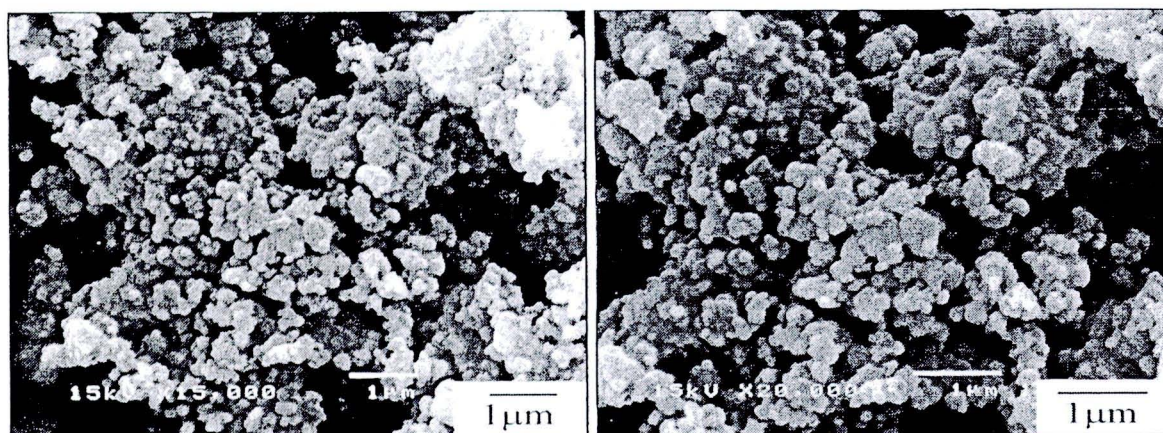
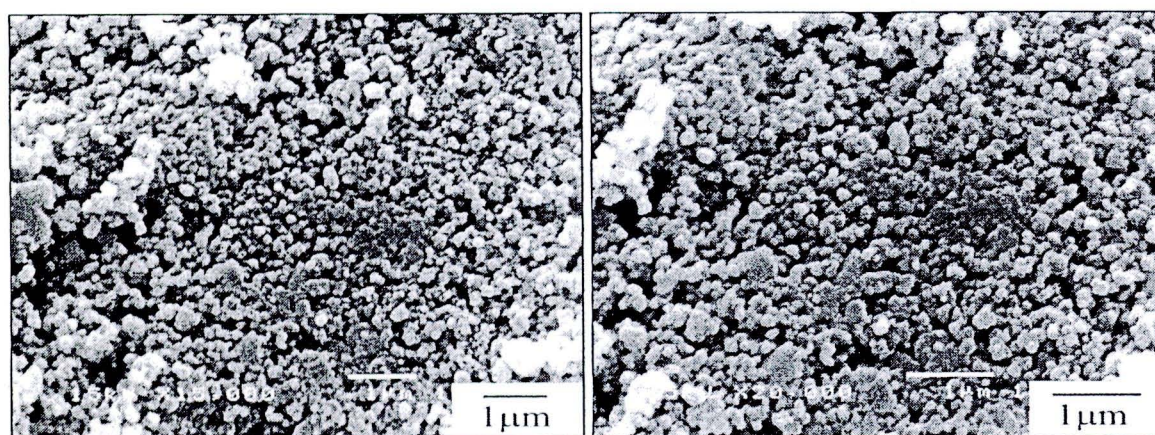


Figure 4.2 Adsorption/desorption isotherm of zinc oxide powder synthesized with the addition of ammonia in the amount of 0%, 7%, and 28% by weight of the solution. All products were calcined at 500°C for 2 hours.

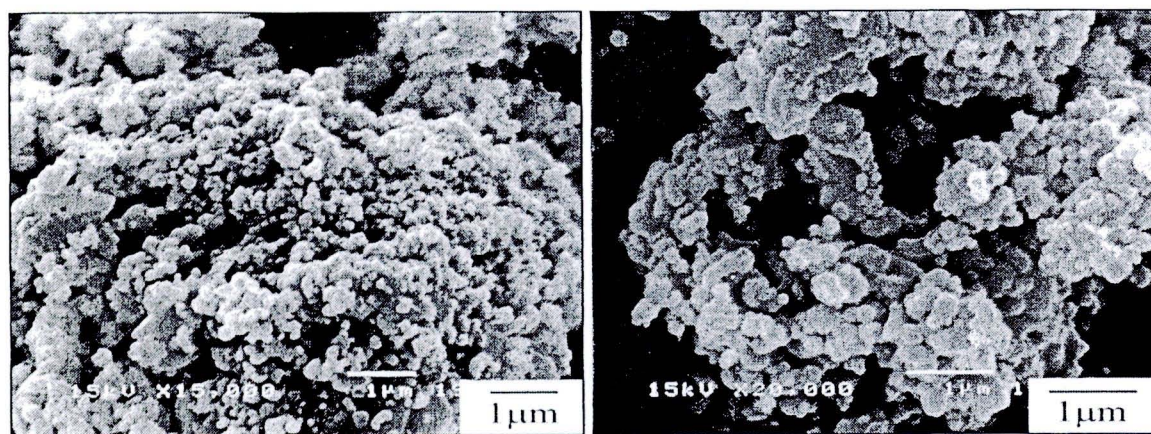
Figure 4.3 shows SEM images of the synthesized ZnO powders ammonia treated with various mass fraction of ammonia solution after calcined at 500°C for 2 hours. The ZnO powders synthesized without ammonia as shown in Figure 4.3(a) were agglomerated with average particle size 175 nm. The increasing ammonia content led to the decrease in particle size as shown in Figure 4.3(b). The average particle size in the powder was 138 nm. The particles were uniform. As Figure 4.3(c) the particles were agglomerated with average size diameter 175 nm.



(a)



(b)



(c)

Figure 4.3 SEM micrographs of the zinc oxide powder synthesized with the use of ammonia at various content: (a) 0% NH_3 (b) 7% NH_3 and (c) 28% NH_3 , after calcined at 500°C for 2 hours.

TG/DTA results for the ZnO powder, after calcined at 500°C for 2 hours (heating rate of 10°C/min), heated from 0-1000°C in flowing air are shown in Figure 4.4. It is clearly seen that the TGA curve indicates no weight loss while neither exothermic nor endothermic peaks are found in the DTA curve. This suggests that calcinations temperature of 500°C is enough for complete combustion of organic. The results confirm that the synthesized ZnO had no residual organics compound within the powder.

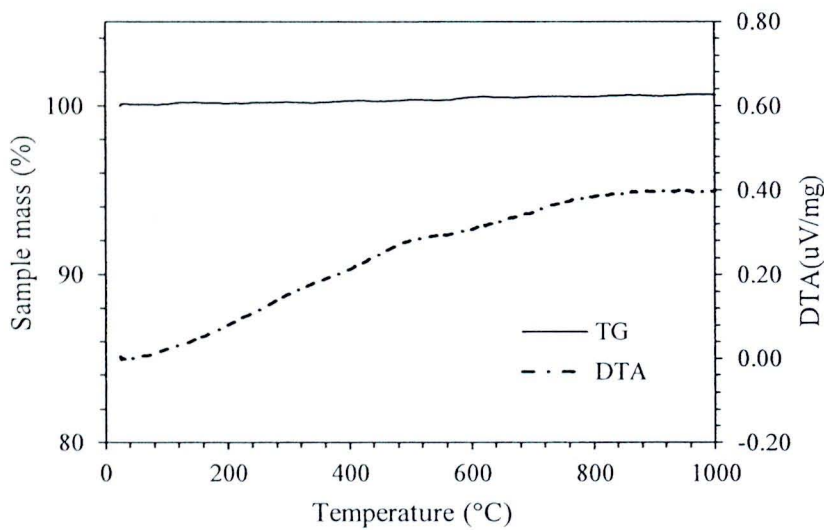


Figure 4.4 TG/DTA curves of the synthesized zinc oxide powder after calcined at 500 °C for 2 hours (heating rate of 10°C/min) without ammonia content.

4.1.2 Synthesized titania

Titania was synthesized by the sol-gel method. During the synthesis, the titania powder was treated with ammonia solution at mass fraction of 0%, 7%, and 28% for 24 hours followed by calcination at 500°C for 2 hours. The phase composition of titania powder after calcination was identified by XRD. XRD patterns of the titania are shown in Figure 4.5. It is confirmed that the product obtained is titania in anatase phase without contamination of rutile phases or other phases relating to nitrogen. The average crystallite size, calculated by the Scherrer equation based on the anatase (101) diffraction peak are shown in the Table 4.2.

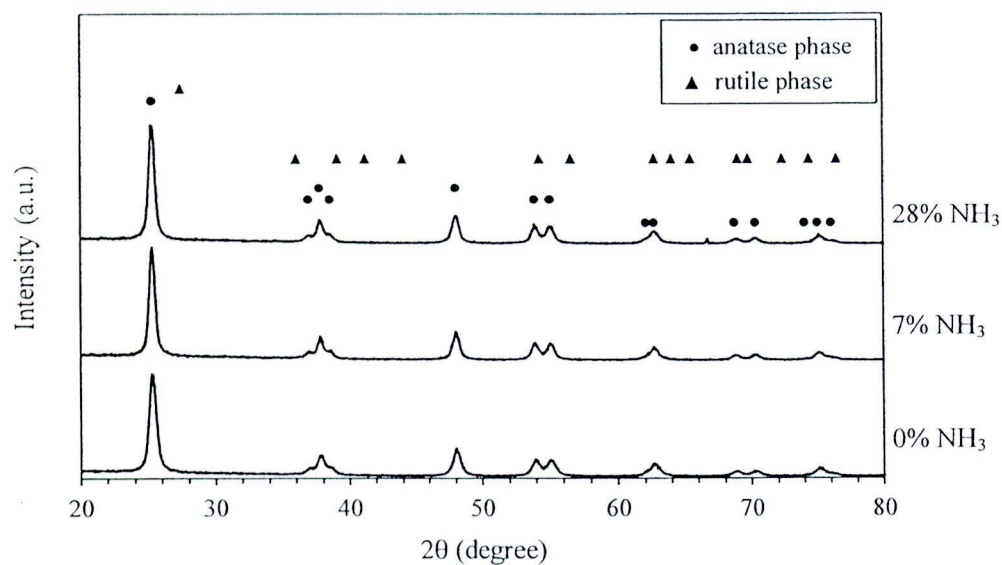


Figure 4.5 XRD patterns of the titania powder synthesized by treated with ammonia solution at the mass fraction of 0%, 7%, and 28% for 2 hours followed by calcination at 500°C for 2 hours.

Table 4.2 Crystallite size and surface area of synthesized titania.

Condition of ammonia added in the solution	Crystallite size, (nm)	Specific surface area, S_{BET} , (m^2/g)	Average pore diameter (nm)	Band gap (eV)
0%	14	36	5	3.30
7%	17	45	4	3.27
28%	16	52	4	3.25

The analysis of the catalyst surface via nitrogen adsorption revealed type IV adsorption/desorption isotherm with a hysteresis loop for the synthesized titania, which indicated the presence of mesopores in the catalyst as shown in Figure 4.6. The calculated specific surface areas based on BET model are also shown in Table 4.2. As the ammonia content was increased from 0% to 28%, the surface area of TiO_2 powder increased from 36 to 52 m^2/g . The results were in good agreement with SEM images.

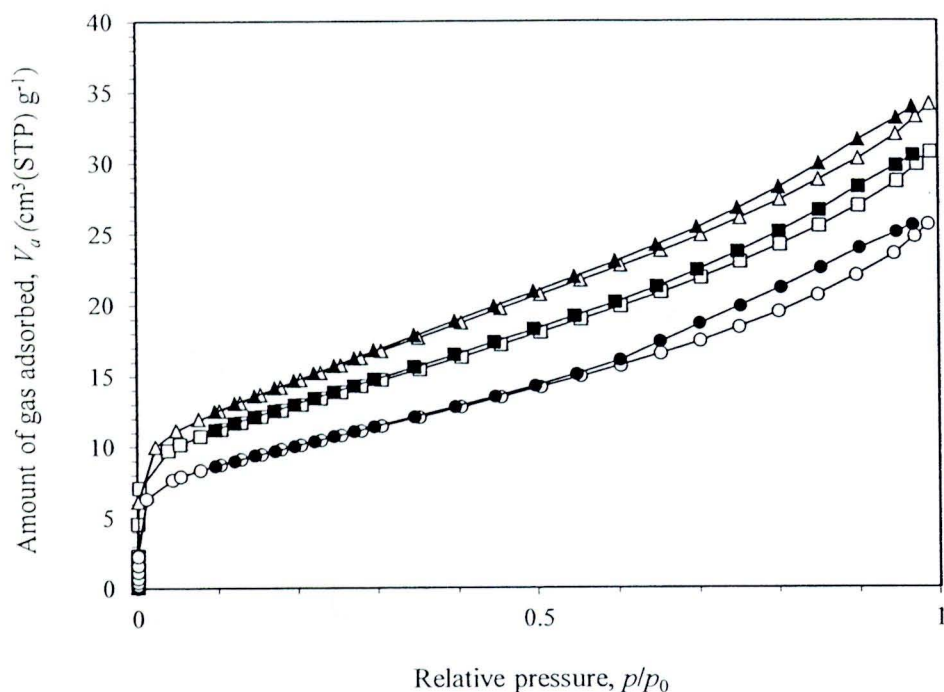
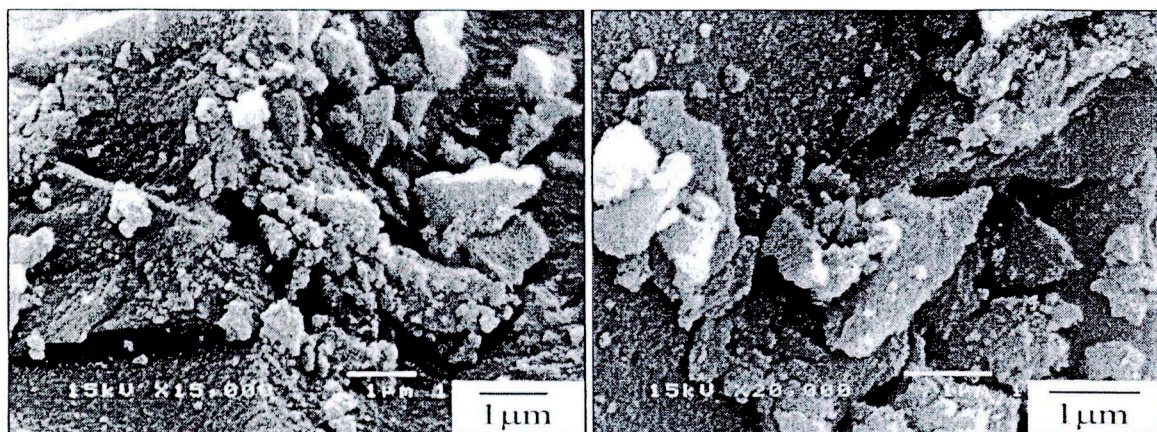
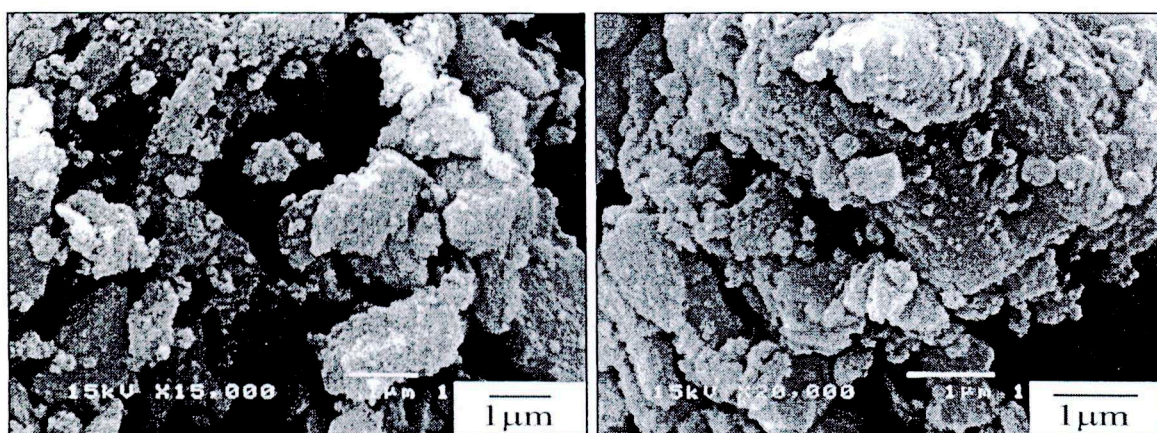


Figure 4.6 Adsorption/desorption isotherm of titanium dioxide powder synthesized with the addition of ammonia in the amount of 0%, 7%, and 28% by weight of the solution. All products were calcined at 500°C for 2 hours.

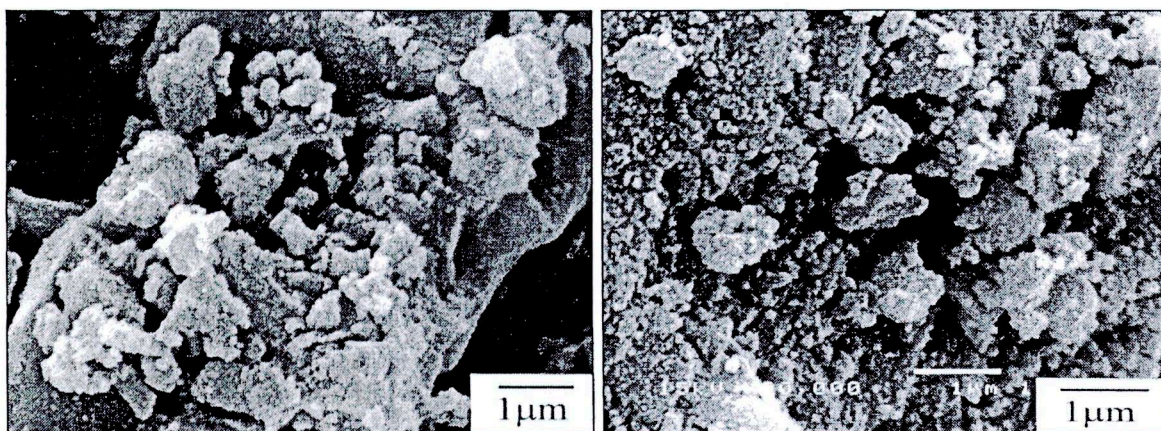
The synthesized TiO_2 powders are consisted of both large and small particles with a wide range of size distribution as shown in Figure 4.7. The powders are consisted of non-spherical particles that are high agglomerated. The aggregation could be due to the high viscosity of the sol, which reduces the dispersion of particles [33]. According to Figure 4.7, the surfaces of the TiO_2 powders become rougher when the content of ammonia used is increased. The particles are highly porous with high surface area which may have higher adsorption affinity towards diuron molecules filled in the pores and can play a role in enhancing the photocatalytic activity of titania particles.



(a)



(b)



(c)

Figure 4.7 SEM micrographs of the synthesized TiO_2 powders synthesized using ammonia at various contents: (a) 0% NH_3 (b) 7% NH_3 and (c) 28% NH_3 , after calcined at 500 °C for 2 hours.

TG/DTA results for the TiO_2 powder, after calcined at 500°C for 2 hours (heating rate of $10^\circ\text{C}/\text{min}$), heated from 0 - 1000°C in flowing air are shown in Figure 4.8. The TGA curve indicates no weight loss, while the DTA curve shows no significant thermal event. The results confirm that TiO_2 powder had no residual organics compound within the powder.

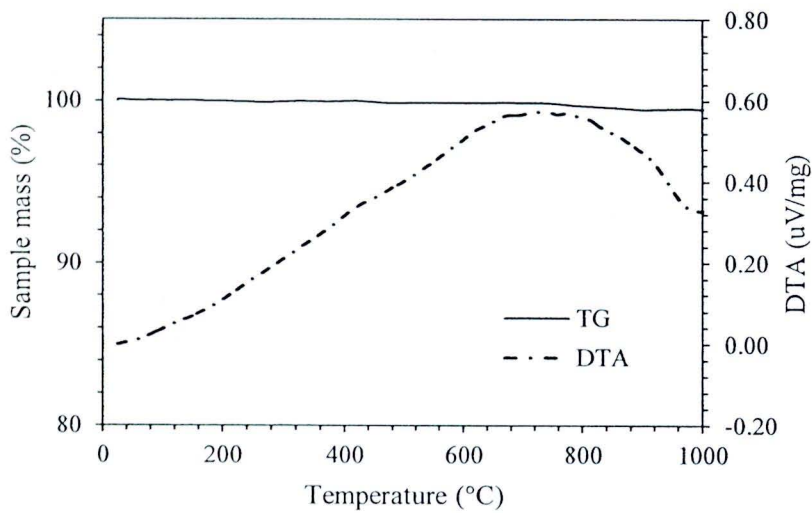


Figure 4.8 TG/DTA curves of the synthesized titanium dioxide powder after calcined at 500°C for 2 hours (heating rate of $10^\circ\text{C}/\text{min}$) without ammonia content.

4.2 Adsorption of Diuron onto the Catalysts

4.2.1 Adsorption isotherm

In this part, diuron was adsorbed onto the catalyst without illumination. Figure 4.9 and Figure 4.10 show the results of the adsorption of diuron onto zinc oxide and titanium dioxide as a function of time at room temperature (27-30°C). The initial concentration of diuron was varied from 1, 5, 10, 15, to 20 ppm respectively. The catalyst loading was 1 mg per 1 ml of the diuron solution. The results confirm that the adsorption takes place very fast, with the adsorption equilibrium occurring after 30 min at low concentration of 1, 5, and 10 ppm while, at the concentration of 15 and 20 ppm, the adsorption equilibrium is reached after 120 min. The amount of diuron adsorbed increased with increasing the concentration of diuron, especially at 20 ppm. Molecules of diuron have more chances to react with catalyst when concentration of diuron is increased. They were adsorbed on the surface of the catalyst better. It might be ascribed to increasing in the driving force of concentration gradient. Therefore the amount of diuron adsorbed increased. The sorption ability of a surface can be measured by the adsorption isotherm. The adsorption isotherm is characterized by the amount of diuron adsorbed per gram of catalysts (ZnO or TiO₂) at equilibrium. The adsorption isotherm of diuron on synthesized ZnO, synthesized TiO₂, commercial ZnO, and commercial TiO₂ at room temperature (27-30°C) are shown in Figure 4.11. The amount of diuron adsorbed at equilibrium increases with the concentration of diuron for all catalysts.

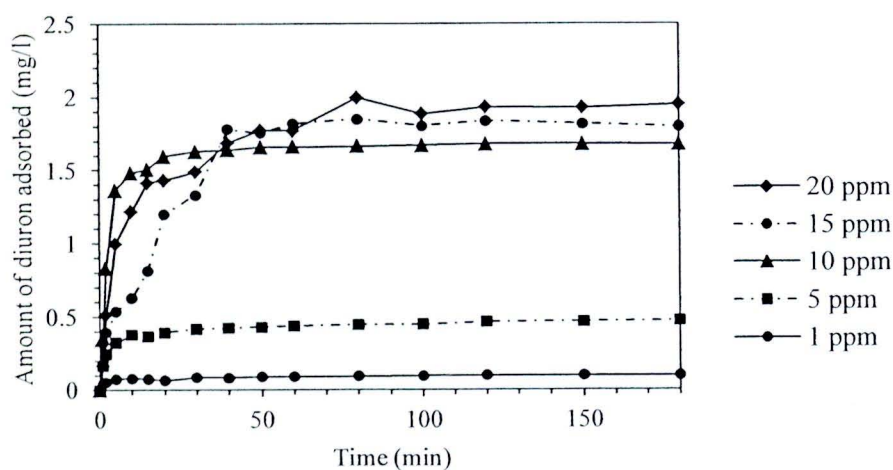


Figure 4.9 Adsorption of diuron on ZnO at room temperature (27-30°C). The initial diuron concentration was 1, 5, 10, 15, and 20 ppm, respectively.

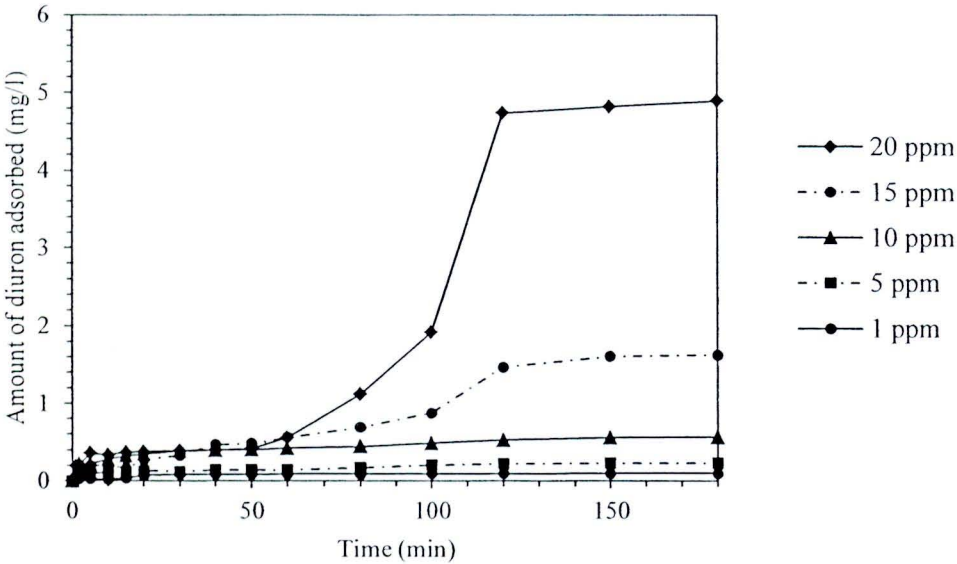


Figure 4.10 Adsorption of diuron on TiO_2 at room temperature (27-30°C). The initial diuron concentration was 1, 5, 10, 15, and 20 ppm, respectively.

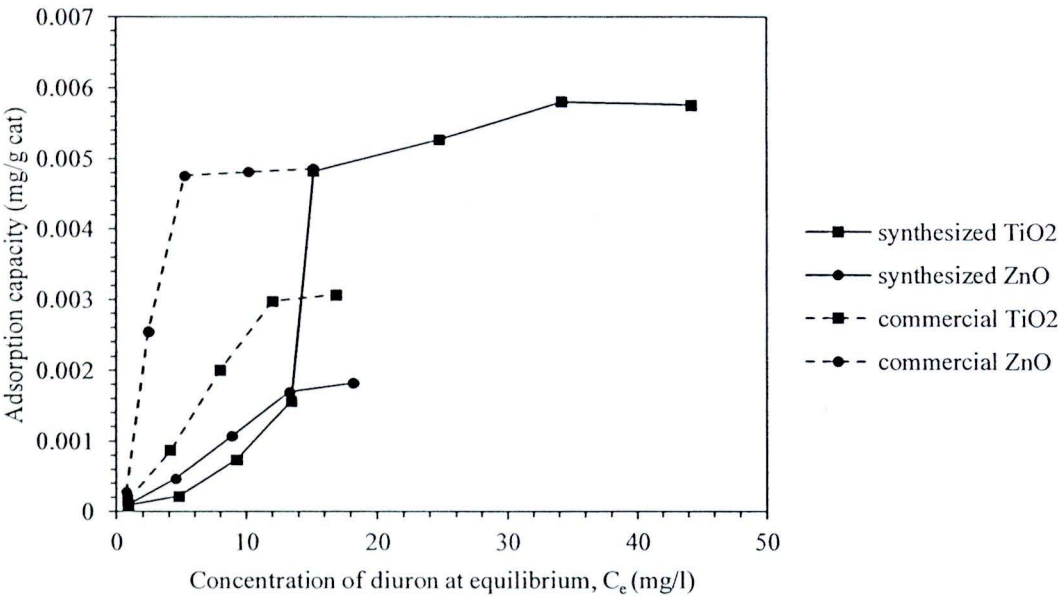


Figure 4.11 Adsorption isotherm of diuron onto synthesized ZnO , synthesized TiO_2 , commercial ZnO , and commercial TiO_2 at room temperature (27-30°C).

Several models have been developed to define the adsorption isotherm. Among them, the isotherms according to Langmuir and Freundlich models have been often considered. According to the linearized form of the Langmuir isotherm model [36, 45, 46]:

$$\frac{1}{q_e} = \frac{1}{q_{\max}} + \frac{1}{bq_{\max}} \frac{1}{C_e} \quad (4.2)$$

where q_e is amount of adsorbate on adsorbent at equilibrium (mg/g), q_{\max} is maximum adsorption capacity (mg/g), C_e is equilibrium concentration (mg/l), and b is constant related to energy of the sorption system (l/mg). For Freundlich model, its linearized form of isotherm [36, 46, 47] is given by Equation 4.3 as follows:

$$\ln q_e = \ln K_f + \frac{1}{n} \ln C_e \quad (4.3)$$

where $\frac{1}{n}$ is adsorption intensity and K_f is Freundlich constant related to adsorption capacity (mg/g(mg/l)^{-1/n}). Figure 4.12 and Figure 4.13 show Langmuir isotherm and Freundlich isotherm for the adsorption of diuron on zinc oxide and titanium dioxide while the value of q_{\max} , b , K_f , n , and R^2 value obtained from the curves of Figure 4.12 and 4.13 are summarized in Table 4.3.

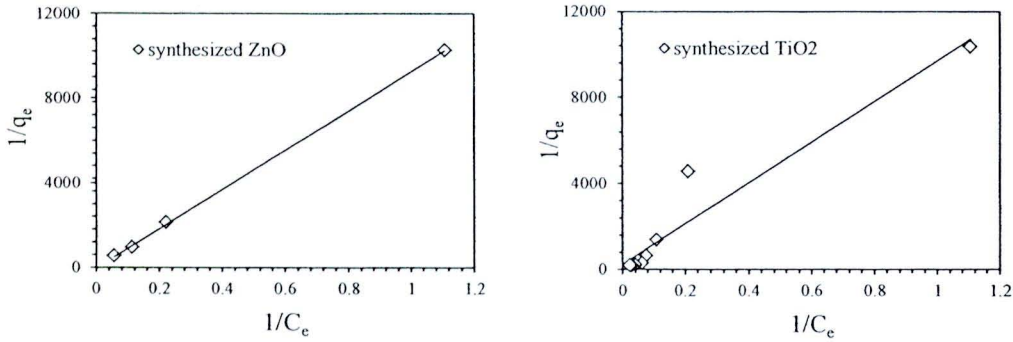


Figure 4.12 Langmuir isotherm for adsorption of diuron on synthesized ZnO and synthesized TiO₂.

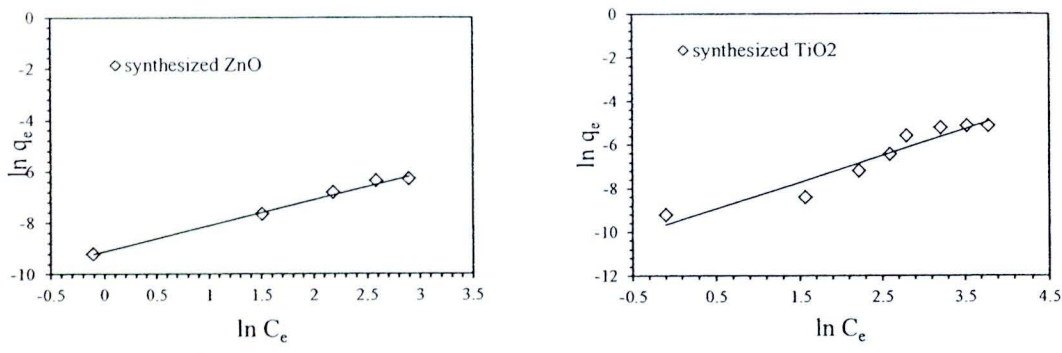


Figure 4.13 Freundlich isotherm for adsorption of diuron on synthesized ZnO and synthesized TiO₂.

Table 4.3 Constants of Langmuir and Freundlich isotherm model for adsorption of diuron on synthesized ZnO and synthesized TiO₂.

Model	Parameters	Values	
		synthesized ZnO	synthesized TiO ₂
Langmuir isotherm model	q_{max}	0.0030	0.0038
	b	0.0348	0.0277
	R^2	0.9974	0.9313
Freundlich isotherm model	K_f	10.8×10^{-5}	7.21×10^{-5}
	n	0.9819	0.8237
	R^2	0.9932	0.9194

Freundlich’s parameter relates to the mean energy of adsorption. A very weak adsorbent/adsorbate interaction occurs at values of n lower than 1, while values higher than 1 suggest a strong adsorbent/adsorbate interaction. At value of n equal to 1 it is assumed that all sites are energetically similar [36, 39]. In our case, value of n lower than 1 for adsorption of diuron on TiO₂ indicated a weak diuron and catalyst interaction and value of n equal to 1 for adsorption of diuron on ZnO indicated all sites are energetically similar. This was confirmed by the values of Freundlich’s constant, K_f , which also relates to the adsorption capacity.

For Langmuir’s parameter, to examine the progression of adsorption dimensionless constant, separation factor r was calculated by following equation

$$r = \frac{1}{1 + bC_0} \quad (4.1)$$

Values $r > 1$ represents unfavorable adsorption condition, and values $0 < r < 1$ represents favorable adsorption conditions [45]. In this case, r value is between 0 and 1 (0.7418 and 0.7829 for synthesized ZnO and TiO₂, respectively), suggesting that the sorption is favorable for diuron on ZnO and TiO₂.

However, the experimental data were fitted well with Langmuir model as indicated by the high R² value.

4.2.2 FTIR studies

Figure 4.14 and 4.15 shows FTIR spectra obtained from diuron solution in methanol mixed with ZnO and TiO₂. The characteristic peaks of methanol were 1360, 1396 and 1050 cm⁻¹ corresponding to the O-H vibration [48, 49] and C-O stretching [50]. The characteristic peaks of diuron were 1655 cm⁻¹ corresponding to the N-H bending, at 1527, 1490 1396 cm⁻¹, and 899 cm⁻¹ corresponding to the C=C aromatic ring, C=C vibration, the benzene ring stretching, and meta benzene respectively, at 1027 and 810 cm⁻¹ corresponding to C-N stretching and C-Cl [48, 51]. A band shift of the C=C vibrations (1510 – 1470 cm⁻¹) towards lower wavenumber after interaction, would indicate an electrodonation reduction which add electron density to a system and tend to stabilize cations or electron poor system, to the ring as consequence of the molecule interaction with ZnO or TiO₂ surface.

According to Figure 4.14, absorption band of Zn-O stretching was around 430-550 cm⁻¹ [52] in curve (b). Considering the diuron–ZnO system only small band shifts are observed. This is the result from the fact that diuron adheres to the surface of zinc oxide only through Van der Waals, which is weak intermolecular interaction. Absorption bands of the C=C vibration and that of the C=C aromatic ring shift from 1490 and 1527 cm⁻¹ toward lower wavenumbers of 1485 and 1513 cm⁻¹, respectively, while the absorption band of C-Cl shift towards higher wavenumber (from 810 to 830 cm⁻¹).

In the diuron – TiO₂ system, only small band shifts are observed as well. In Figure 4.15, the broad band between 500 and 600 cm⁻¹ correspond to Ti-O band [53, 54]. The shifting in the absorption band of C=C aromatic ring (from 1527 to 1515 cm⁻¹) and C=C vibration (from 1490 to 1485 cm⁻¹) are similar to those observed in diuron – ZnO system, which also indicates an electrodonation reduction to the ring as consequence of the molecule

interaction with TiO_2 surface. Absorption band of CH_3 group was shift towards higher wavenumber (from 1037 to 1048 cm^{-1}).

However, the results indicated only small shift, it should be noted that, the adsorption of diuron on TiO_2 and ZnO are physisorption (Van der Waals and electrostatic forces). The structures have not change. This suggest, the reaction could not be occurs without UV irradiation.

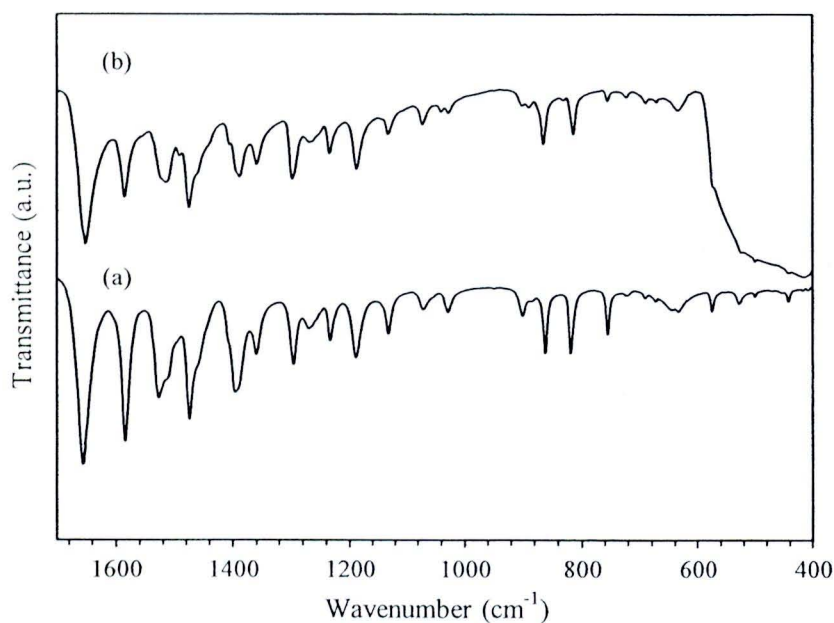


Figure 4.14 FTIR spectrum obtained from (a) diuron solution in methanol, (b) diuron solution in methanol mixed with ZnO for 180 min.

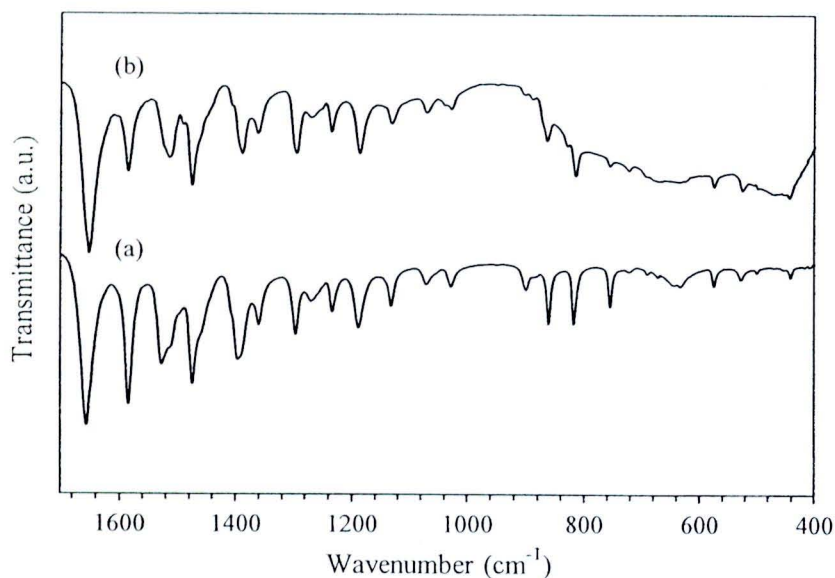


Figure 4.15 FTIR spectrum obtained from (a) diuron solution in methanol, (b) diuron solution in methanol mixed with TiO_2 for 180 min.

4.3 Photodegradation of Diuron

Conventionally, it has been reported that the photocatalytic system produces hydroxyl radical during the reaction. The radical is a strong oxidizing agent that reacts with diuron and causes its degradation [1]. Degradation of diuron can be expressed by the following reaction [55].



The complete mineralization expressed by the following equation [1, 55]:



In this work, the photodegradation of diuron aqueous solution was conducted in a pyrex reactor. The content of the photocatalyst was kept at 1 mg of the catalyst per 10 ml of the solution (initial diuron concentration of 10 ppm). The photodegradation of diuron solution using zinc oxide or titania as a catalyst was achieved within 6 hours of UV irradiation. The experiments under UV-light without catalyst, confirmed the absence of photolysis of diuron

as shown in Figure 4.16. Figure 4.16 describe the relative decrease in concentration of diuron as a function of irradiation time in the presence of catalysts, i.e. zinc oxide and titania are shown in Figure 4.19 It can be inferred that, there is no appreciable degradation when the aqueous solution is irradiated in the absence of titania or zinc oxide. The degradation of diuron is less than 5% after 6 hours of irradiation without the catalyst, which is similar to the result reported for self-degradation in the dark at room temperature indicating that hydrolysis of diuron can be neglected [56]. The enhanced degradation by the UV/photocatalyst suggests that both UV light and photocatalyst are required for efficient degradation of diuron.

4.3.1 Photodegradation of diuron on zinc oxide

Diuron is degraded in less than 360 minutes in the presence of zinc oxide. Concentration of diuron with respect to the initial diuron concentration (C/C_0) during the photocatalytic degradation on zinc oxide prepared using various mass fractions of ammonia is shown in Figure 4.16. The results reveal that the activity of zinc oxide increases when the higher amount of ammonia is used during preparation. The conversion obtained from zinc oxide powder ammonia-treated with NH_3 mass fraction of 28% is evidently the highest value, while in the case of zinc oxide without ammonia treatment the lowest conversion is achieved. Thus, the photocatalytic behavior of zinc oxide powder depends upon the ammonia treating process. It is found that diuron is degraded by about 92, 96, and 98%, when zinc oxide treated with ammonia at the fraction of 0, 7, and 28% is used, respectively.

According to many researchers, the photocatalytic degradation of organic pollutants is described by the pseudo-first order kinetics.

$$r = -\frac{dC}{dt} = k_{app}C \quad (4.4)$$

where r is the rate of diuron degradation, C is the concentration of diuron, t is the irradiation time, k_{app} is the apparent rate constant of a pseudo first order reaction [37, 57]. After integration, Equation 4.4 can be simplified to Equation 4.5 where C_0 is the initial concentration of diuron.

$$\ln\left(\frac{C_0}{C}\right) = k_{app}t \quad (4.5)$$

Kinetic studies were assessed by monitoring the change in diuron concentration at certain interval of time (C). The apparent first order rate constants (k_{app}) were determined by employing Equation 4.5 using the plot of $\ln(C_0 / C)$ versus irradiation time t as shown in Figure 4.17. The k_{app} was determined by calculating the slope of the line obtained. The resulting first order rate constant for each catalyst is shown in Table 4.3. The R^2 values are between 0.9878 and 0.9983. The degradation curve can be fitted reasonably well by an exponential decay curve suggesting the pseudo first order kinetics.

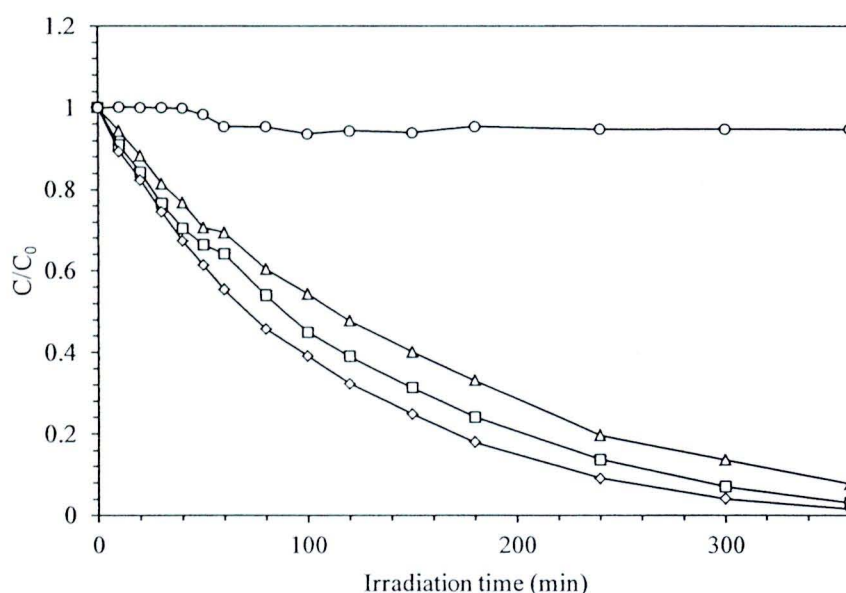


Figure 4.16 Concentration of diuron with respect to the initial diuron concentration (C/C_0) during the photocatalytic degradation on zinc oxide at various mass fraction of ammonia: \triangle : 0% NH_3 , \square : 7% NH_3 , \diamond : 28% NH_3 , and \circ : without catalyst. The reaction was conducted using 1 mg of zinc oxide per 10 ml of solution and using the initial concentration of diuron is 10 ppm.



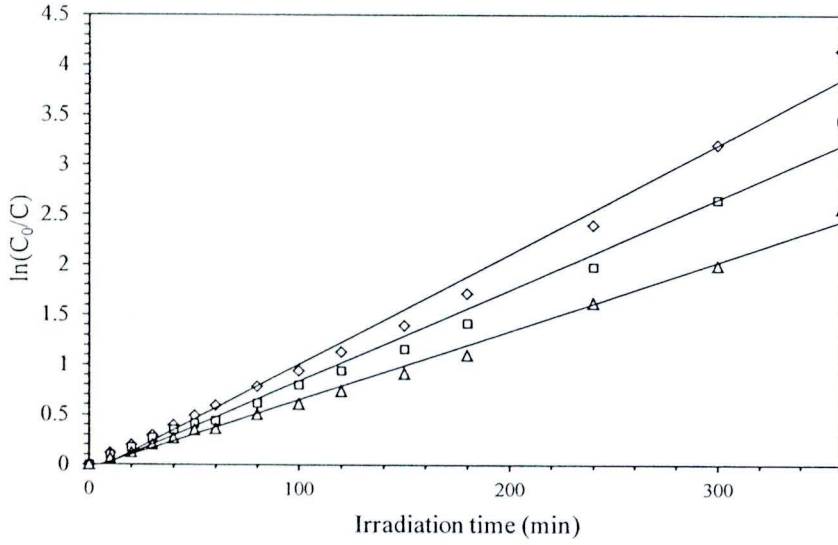


Figure 4.17 First –order linear transforms of the photocatalytic degradation on zinc oxide at various mass fraction of ammonia: \triangle : 0% NH_3 , \square : 7% NH_3 , and \diamond : 28% NH_3 . The reaction was conducted using 1 mg of zinc oxide per 10 ml of solution and using the initial concentration of diuron is 10 ppm.

The Langmuir-Hinshelwood (L-H) kinetics is the most commonly used kinetic expression to explain the kinetics of the heterogeneous catalytic processes.

$$r = -\frac{dC}{dt} = k_r \theta = \frac{k_r KC}{1 + KC} \quad (4.6)$$

where k_r is the true rate constant and K is the constant of adsorption equilibrium of Langmuir – Hinshelwood [37]. When the solution is highly diluted, the term KC can be neglected. Previously several researchers approximated the Langmuir-Hinshelwood kinetics to the first order by assuming the term $KC \ll 1$ [37, 38]. Thus the Langmuir-Hinshelwood kinetics expression can be written as Equation 4.7. The constants k_r and K can be calculated from the corresponding integrated expression in Equation 4.8.

$$r = -\frac{dC}{dt} = k_r KC \quad (4.7)$$

$$\ln\left(\frac{C_0}{C}\right) + K(C_0 - C) = k_r Kt \tag{4.8}$$

The data shown in Figure 4.16 were fitted against the Langmuir – Hinshelwood kinetics model (Equation 4.8). The predicted k_r and K according to the Langmuir-Hinshelwood kinetics are shown in Table 4.4. The results show that describes a linear behavior and the R^2 values are comprised between 0.9968 and 0.9976. This clearly indicates that the photodegradation reaction of diuron follows the pseudo first order kinetics. Experimental data show that the photodegradation of diuron by using zinc oxide as the catalyst is consistent with the Langmuir-Hinshelwood model.

Table 4.4 The apparent rate constant (k_{app}), reaction rate constants (k_r), and the adsorption constant (K) for the photocatalytic degradation of diuron using zinc oxide at various mass fraction of ammonia.

%NH ₃	Pseudo first-order model		Langmuir-Hinshelwood model		
	$k_{app}(\text{min}^{-1})$	R^2	$k_r(\text{ppm/min})$	$K(\text{min}^{-1})$	R^2
0%	0.0067	0.9935	0.1881	0.0439	0.9976
7%	0.0092	0.9983	0.1745	0.0656	0.9976
28%	0.0106	0.9878	0.2073	0.0634	0.9968

The decrease of TOC (Total Organic Carbon) as a result of mineralization of diuron was also observed during the degradation process. Figure 4.18 shows the depletion in TOC as a function of time on irradiation of an aqueous solution of diuron (10 ppm of diuron in the presence of zinc oxide 1 mg per 10 ml). It is found that, 49%, 40%, and 55% mineralization of diuron takes place after 360 min of irradiation by zinc oxide with ammonia mass fraction of 28%, 7%, and 0%, respectively. The plot between TOC vs. reaction time, indicates that organics intermediates are produced in the course of the photodegradation process. After the reaction time of 12 hours, it is found that the total organic carbon of the solution is lower than the detection limit of the TOC analyzer.

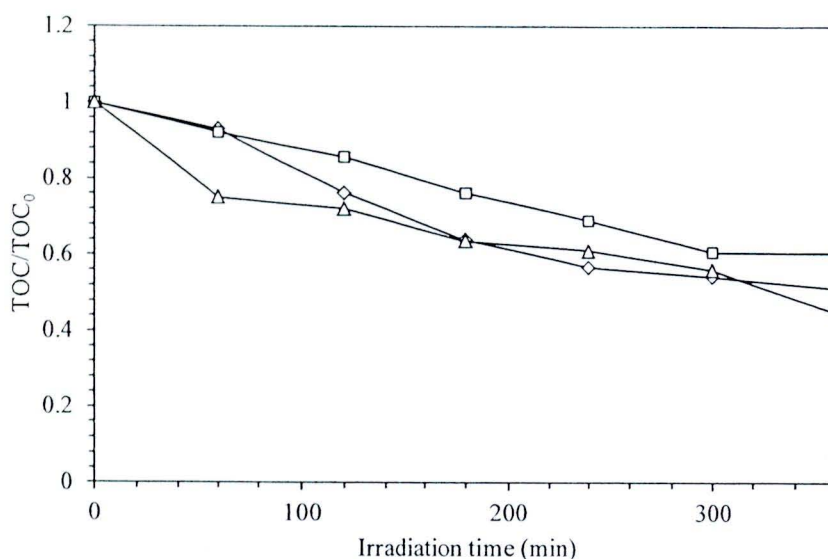


Figure 4.18 Total organic carbon (TOC) with respect to the initial TOC of diuron solution (TOC/TOC_0) during the photocatalytic degradation on zinc oxide at various mass fraction of ammonia: \triangle : 0% NH_3 , \square : 7% NH_3 , and \diamond : 28% NH_3 . The reaction was conducted using 1 mg of zinc oxide per 10 ml of solution and using the initial concentration of diuron is 10 ppm.

4.3.2 Photodegradation of diuron on titania

Figure 4.19 shows the disappearance of diuron by photocatalytic degradation using the synthesized titania as the catalyst, concentration of diuron with respect to the initial diuron concentration (C/C_0) during the photocatalytic degradation on titania at various mass fraction of ammonia. The results indicate that the activity of titania is increased when the ammonia mass fraction is increased. At ammonia mass fraction of 0, 7, and 28%, it is found that diuron is degraded by about 21, 33, and 45%, respectively. The transformed first order plots (Equation 4.5) are giving in Figure 4.20. The apparent rate constant can be determined from the slope of curve in Figure 4.20, obtained as shown in Table 4.5. It is observed that the first order kinetics does not provide good fit to the experimental data for all condition of ammonia mass fraction. The data shown in Figure 4.19 are fitted against the Langmuir – Hinshelwood kinetic model (Equation 4.8). The results are shown in Table 4.5. Experimental data show that the photodegradation of diuron on titania is inconsistent with the Langmuir-Hinshelwood model because R^2 value does not approach to 1.

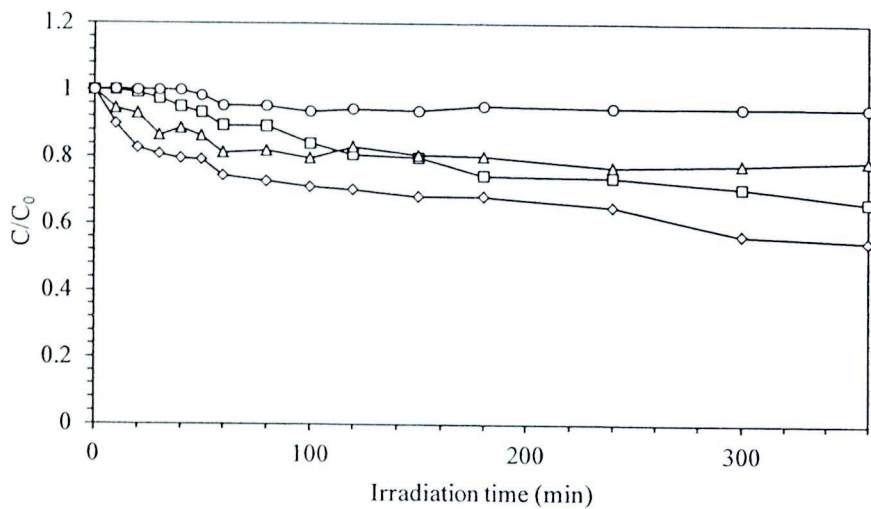


Figure 4.19 Concentration of diuron with respect to the initial diuron concentration (C/C_0) during the photocatalytic degradation on titania at various mass fraction of ammonia: \triangle : 0% NH_3 , \square : 7% NH_3 , \diamond : 28% NH_3 , and \circ : without catalyst. The reaction was conducted using 1 mg of titania per 10 ml of solution and using the initial concentration of diuron is 10 ppm.

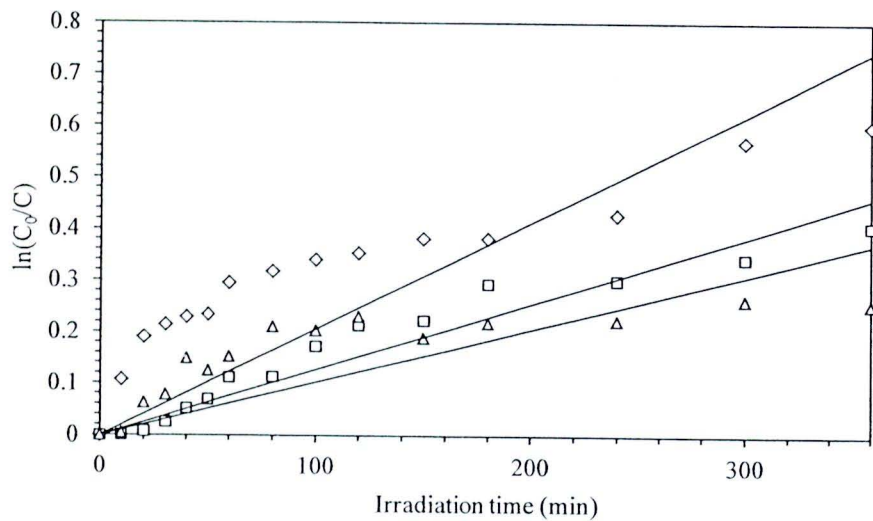


Figure 4.20 First-order linear transforms of the photocatalytic degradation of diuron on titania at various mass fraction of ammonia: \triangle : 0% NH_3 , \square : 7% NH_3 , and \diamond : 28% NH_3 . The reaction was conducted using 1 mg of titania per 10 ml of solution and using the initial concentration of diuron is 10 ppm.

Table 4.5 The apparent rate constant (k_{app}), reaction rate constants (k_r), and the adsorption constant (K) for the photocatalytic degradation of diuron using titania at various mass fraction of ammonia.

%NH ₃	Pseudo first-order model		Langmuir-Hinshelwood model		
	$k_{app}(\text{min}^{-1})$	R ²	$k_r(\text{ppm/min})$	$K(\text{min}^{-1})$	R ²
0%	0.0010	0.7783	0.9992	0.0048	0.7716
7%	0.0013	0.7794	0.0001	0.0470	0.7405
28%	0.0021	0.8847	0.2689	0.0080	0.9178

Figure 4.21 shows the depletion in TOC (Total Organic Carbon) as a function of time on irradiation of an aqueous solution of diuron (10 ppm of diuron in the presence of titania 1 mg per 10 ml). It is found that, 19%, 7%, and 17% mineralization of diuron takes place after 360 min of irradiation by titania with ammonia mass fraction of 28%, 7%, and 0%, respectively. Variation of ammonia mass fraction in synthesized titania does not much affect the TOC removal. TOC values remain constant during illumination, which indicates that organics intermediates were produced during the photodegradation process. The plot between TOC vs. reaction time, indicates that organics intermediates are produced in the course of the photodegradation process. After the reaction time of 12 hours, it is found that the total organic carbon of the solution is lower than the detection limit of the TOC analyzer.

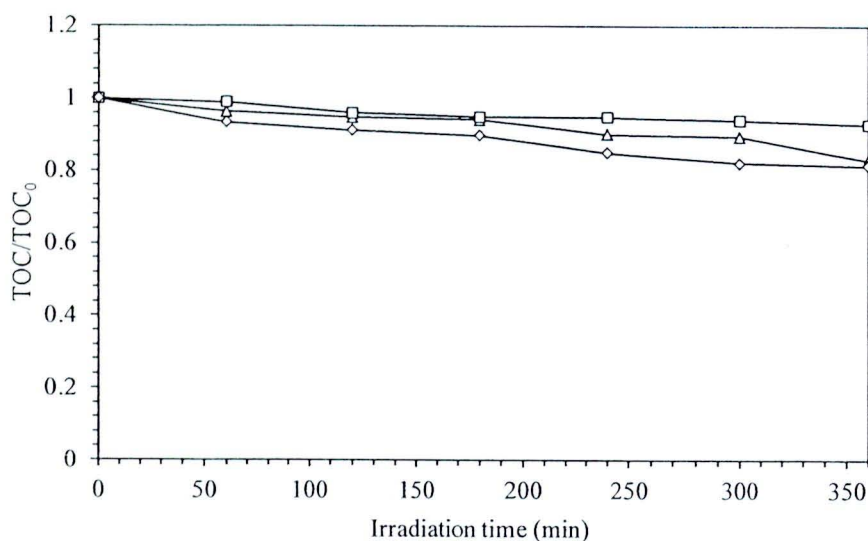


Figure 4.21 Total organic carbon (TOC) with respect to the initial TOC of diuron solution (TOC/TOC_0) during the photocatalytic degradation on titania at various mass fraction of ammonia: \triangle : 0% NH_3 , \square : 7% NH_3 , and \diamond : 28% NH_3 . The reaction was conducted using 1 mg of titanium dioxide per 10 ml of solution and using the initial concentration of diuron is 10 ppm.

Both zinc oxide and titania have been known to be capable of producing of radicals upon the exposure with UV light. However, comparison of the catalytic activities of zinc oxide and titania, in regard of the decrease in both diuron concentration and the total organic carbon in the solution, clearly indicates the difference in the degradation efficiency. It was found that the synthesized zinc oxide has higher performance in degrading and mineralization of diuron than titania, regardless of much lower surface area. Due to the amount of diuron adsorbed at equilibrium by zinc oxide rather than adsorbed by titania. The result of adsorption isotherm showed that the diuron concentration of 10 ppm, the amount of diuron adsorbed at equilibrium using zinc oxide as a catalyst larger than using titania as a catalyst.

4.4 Intermediate Products of the Photodegradation

During the photocatalytic reaction, radicals formed from the photocatalysts react with diuron to generate the intermediates. Structure of functional groups attaching to aromatic ring of diuron is mainly responsible for the structure of the intermediates formed. Diuron clearly offers two sites for the reaction, i.e. the aromatic ring and the aliphatic side chain [58].

4.4.1 Photodegradation on zinc oxide

4.4.1.1 Effect of pH of diuron solution

The effect of pH of the aqueous diuron solution on the photocatalytic degradation was studied. The pH value of the diuron solution was adjusted to the desired value in the range of 3 to 10 by using HCl or NaOH. For the study of this parameter, the amount of zinc oxide powder added into the solution was fixed at the ratio of 1 mg of zinc oxide to 10 ml of the solution. Intermediates were detected by HPLC, during the photocatalytic treatment. In Figure 4.22 - 4.23 and Table 4.6, the extent of photodegradation of diuron is reported for the reaction at pH 3, 7, and 10. The pH of the solution was adjusted before irradiation and it was not controlled during the course of the reaction. The results for the degradation are illustrated in Figure 4.22. The transform first order plots are given in Figure 4.23 whereas the apparent rate constants are shown in Table 4.5. The data shown in Figure 4.22 were fitted against the Langmuir-Hinshelwood kinetic model. The results are shown in Table 4.6.

Table 4.6 shows the apparent rate constant, calculated reaction rate constants and the calculated adsorption constant based on the Langmuir-Hinshelwood kinetic model of the photodegradation of diuron at various pH.

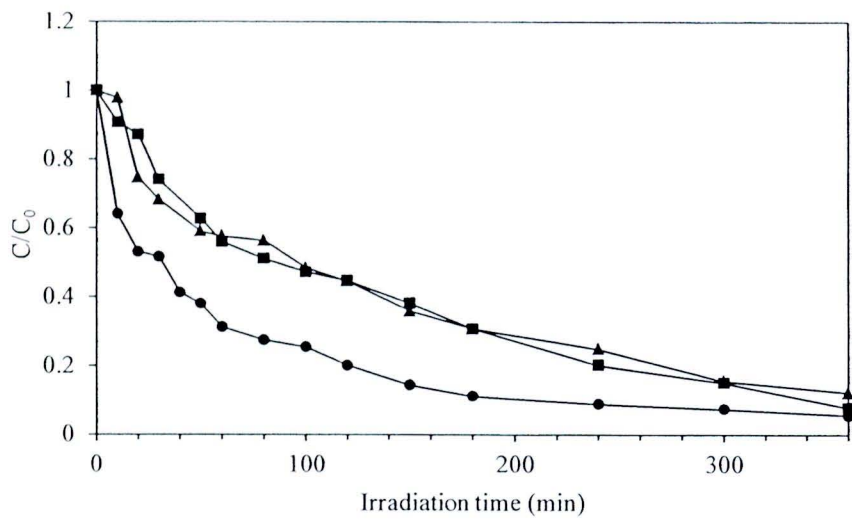


Figure 4.22 Effect of pH of the solution on photodegradation efficiency of diuron. The pH is adjusted at pH 3 (■), pH 7 (●), and pH 10 (▲).

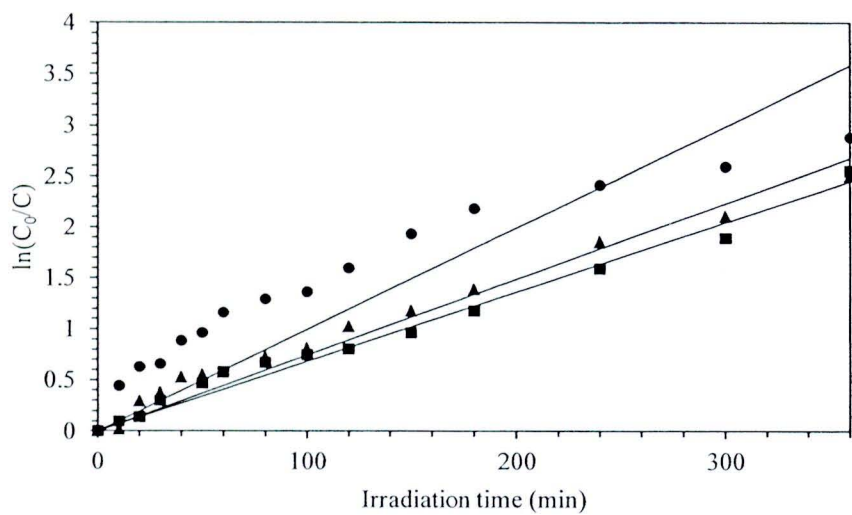
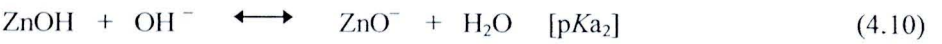
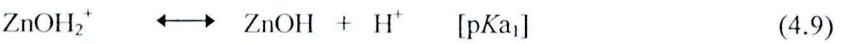


Figure 4.23 First order linear transforms of the photodegradation efficiency of diuron at various pH values. The pH is adjusted at pH 3 (■), pH 7 (●), and pH 10 (▲).

Table 4.6 The apparent rate constant (k_{app}), reaction rate constants (k_r), and the adsorption constant (K) for the photocatalytic degradation of diuron using zinc oxide at various pH of solution.

pH of solution	Pseudo first-order model		Langmuir-Hinshelwood model		
	$k_{app}(\text{min}^{-1})$	R^2	$k_r(\text{ppm/min})$	$K(\text{min}^{-1})$	R^2
3	0.0068	0.9832	0.9999	0.0264	0.8246
7	0.0100	0.7281	0.9999	0.8097	0.8916
10	0.0074	0.9692	0.9995	0.1568	0.7612

The results indicate that the photodegradation of diuron is increased with increasing pH up to pH 7, beyond which the degradation decreases. At pH 3, 7, and 10 it was found that diuron is degraded by about 92, 94, and 91%, respectively. Generally, the effect of pH on organic degradation assisted by the semiconductor oxides has been related to the establishment of acid-base equilibria governing the surface chemistry of metal oxides in water, as shown in the following reactions.



The pH at which the surface of an oxide is uncharged is defined as the point of zero charge (pH_{pzc}). It has been reported that the point of zero charge for zinc oxide is about 9 [18]. The effect of pH on the photocatalytic performance can be explained in terms of electrostatic interaction between the catalyst surface and the target substrate. It is expected that this interaction affects the encounter probability between hydroxyl radical and diuron. The reaction would be enhanced or hindered depending on whether attractive or repulsive forces prevail, respectively. Diuron is negatively charged above its $\text{p}K_a$ (2.68), whereas catalysts are positively charged below $\text{pH} \sim 9$. Optimal conditions were found at $\text{p}K_a < \text{pH} < \text{pH}_{\text{pzc}}$ at which the positive charged zinc oxide and negative charged diuron should attract each other

[18, 29, 59]. Other concomitant effect can come into play. For example ZnO can undergo photocorrosion through self-oxidation.



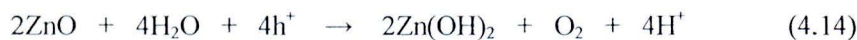
In particular, ZnO powder exhibit tendency to dissolve with decreasing pH (Eq. 4.12) [18].



In a strongly alkaline environment, ZnO can undergo dissolution according to



Moreover, the possible formation of photocatalytically inert Zn(OH)_2 surface layers upon UV irradiation (Eq. 4.14) has also to be considered in aqueous media [18].



Therefore, the reduction of photocatalytic activity of ZnO at exceedingly low and high pH values can originate from either acidic/photochemical corrosion of the catalyst from alkaline dissolution and/or surface passivation with Zn(OH)_2 .

The results regarding the intermediates formed are shown in Figure 4.24-4.26. The total number of intermediates are detected by HPLC from the reaction at pH 3, 7, and 10, are 8, 9, and 9 kinds of intermediates respectively. Concentrations of these intermediates are expected to be very low, since the intensities of the HPLC signals for the intermediates are much lower than that of diuron. It should be noted that, without identification of the intermediate, the standard calibration curve could not be constructed. Consequently, quantitative results of the intermediates were not obtained. Nevertheless, based on the intensity of the signal, it was found that the concentration of the intermediates also changes along the course of the photodegradation.

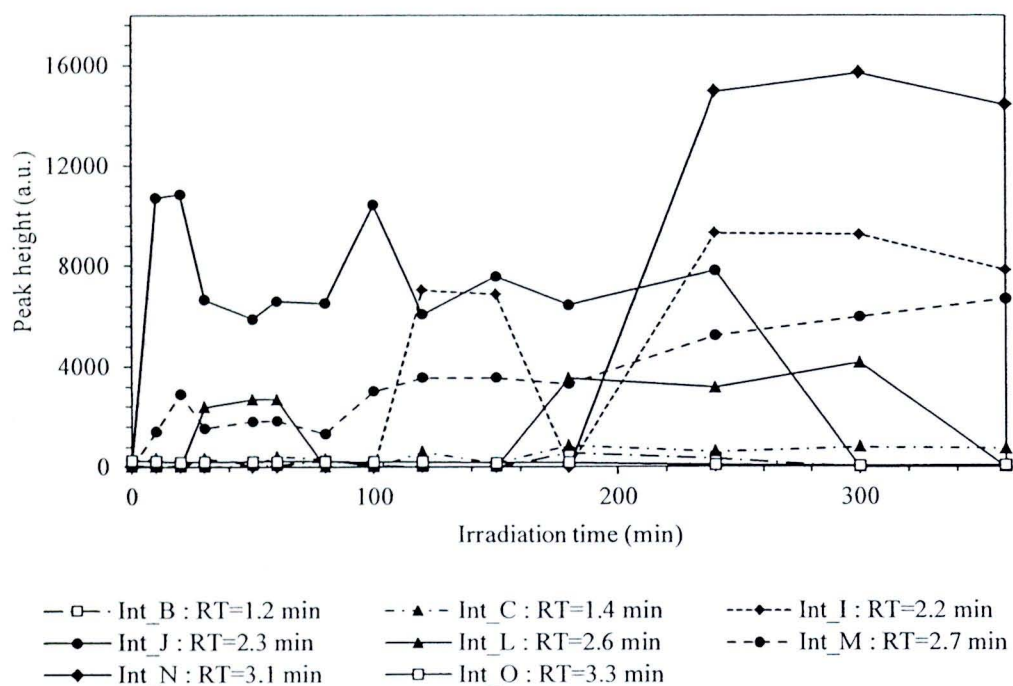


Figure 4.24 HPLC peak height of intermediates generated during photocatalytic degradation on diuron on zinc oxide and the initial pH of 3.

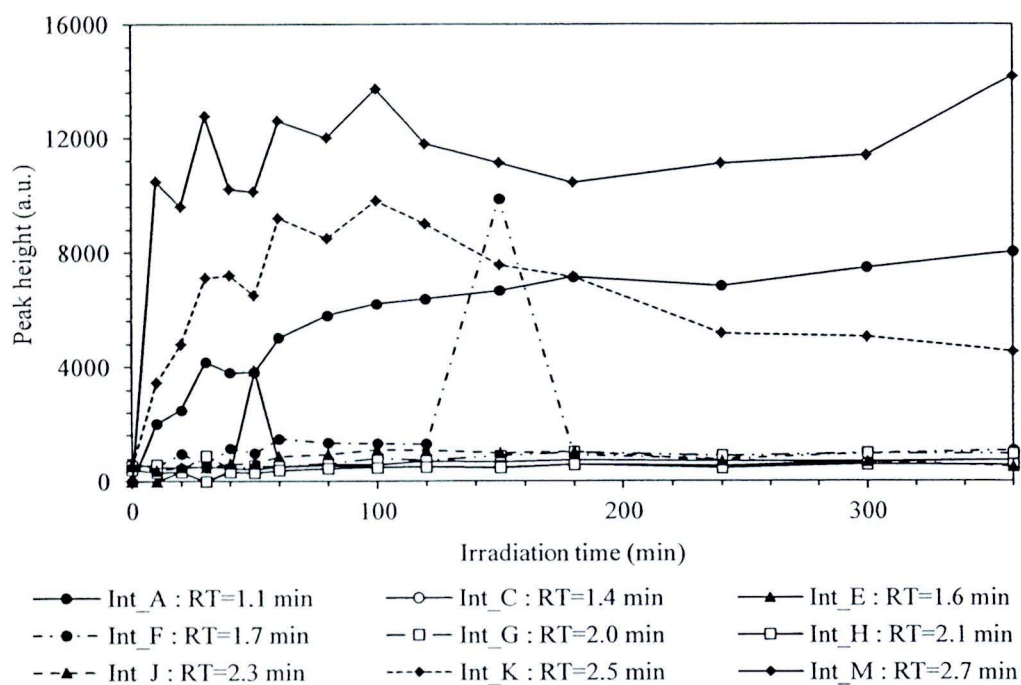


Figure 4.25 HPLC peak height of intermediates generated during photocatalytic degradation on diuron on zinc oxide and the initial pH of 7.

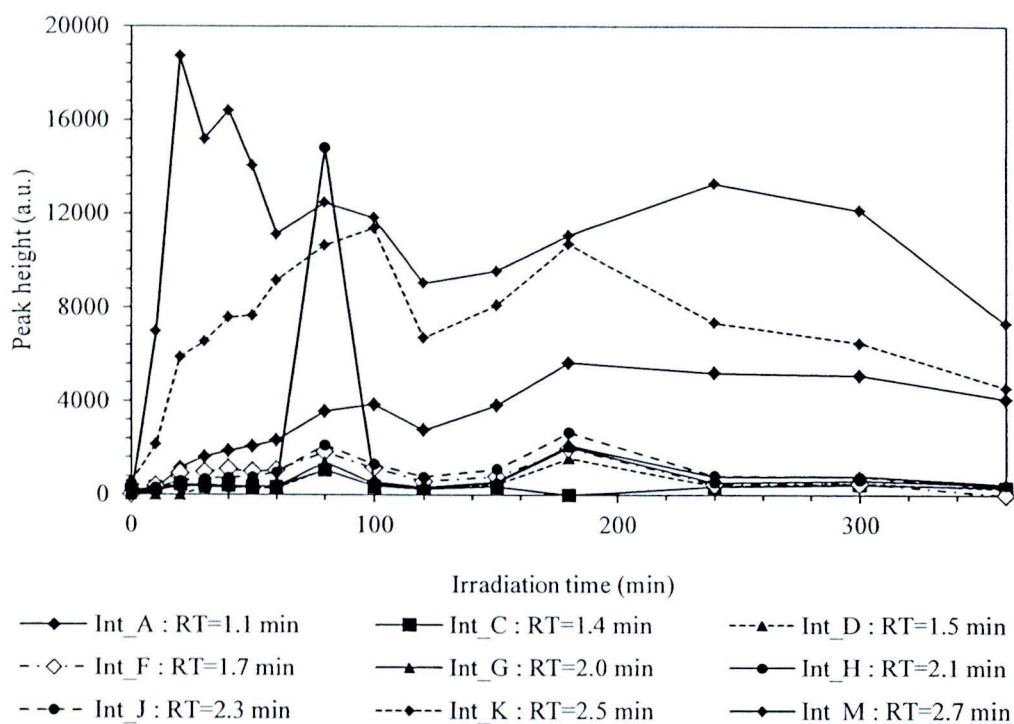


Figure 4.26 HPLC peak height of intermediates generated during photocatalytic degradation on diuron on zinc oxide and the initial pH of 10.

Concentration of most intermediate increase with irradiation time, although the data show some fluctuation. It can be observed that each unknown intermediates are presented at very low concentration. However these small molecules are not detectable by HPLC analysis. The effect of different pH of diuron solution using zinc oxide as catalyst and behavior of intermediates are also compared in Figure 4.24-4.26. It shows that most photodegradation intermediates are formed after 30 minutes of irradiation time. Several intermediates are formed within short time and the concentration of intermediates are high. Some intermediates remain stable at low concentration even after 6 hours of the reaction.

Comparison of the intermediates formed from the reaction at different pH, reveals common intermediates as well as different intermediates. The fact that different pH of the solution produces different combination of reaction intermediates might be the result of charge on the surface of catalyst. Attempts were made to identify the intermediate products through analysis using LC-MS.

Samples collected at different irradiation time were freeze dry for the purpose of concentrating the intermediates. These powders were resuspended in 70% acetonitrile per 30% water and injected into LC/MS. Diuron peak was observed as reported in literature at 231 m/z and 232 m/z in negative and positive detection mode respectively.

Two assumptions were made for the identification process. First, m/z values that were not observed in the mass spectrum of standard diuron were considered to belong to intermediates products derived from diuron. Second, peak of all m/z values reported were considered as pseudo molecular ion peak since at fragmentator voltage of 120 V was used for structural determination of intermediates.

Table 4.7 Possible intermediates generated from photodegradation of diuron on zinc oxide at pH of 3, 7, and 10.

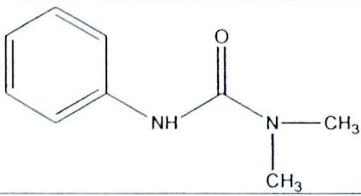
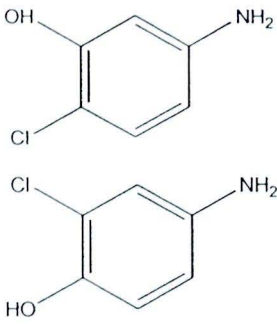
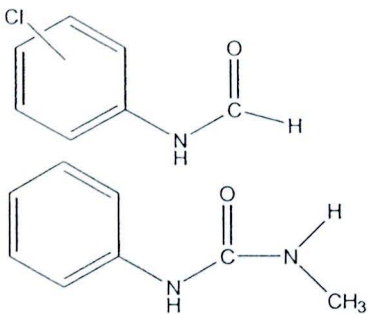
Compound	Propose structure	pH3	pH7	pH10
1 [60]		◆		
2		◆	◆	◆
3 [61]			◆	

Table 4.7 (continued)

Compound	Propose structure	pH3	pH7	pH10
4 [44]		◆	◆	◆
5		◆	◆	
6		◆		
7 [62]		◆	◆	◆
8		◆	◆	
9 [63]				◆
10 [1, 60, 64]		◆	◆	◆

Table 4.7 (continued)

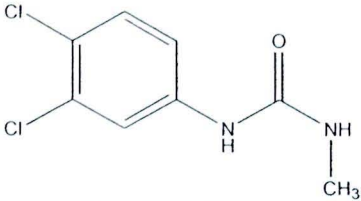
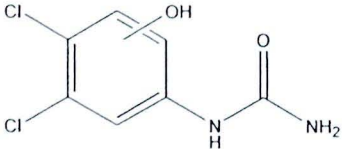
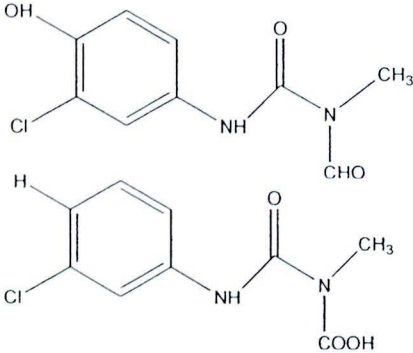
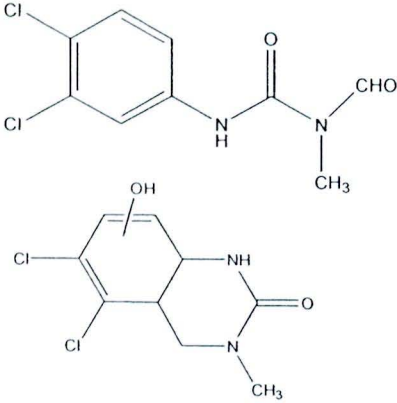
Compound	Propose structure	pH3	pH7	pH10
11 [42, 61, 64]		◆	◆	◆
12			◆	
13			◆	
14 [60, 62, 64, 65]		◆	◆	

Table 4.7 (continued)

Compound	Propose structure	pH3	pH7	pH10
15 [42, 60, 66]	<p>Chemical structure of compound 15: 3,5-dichloro-N-(2-hydroxyethyl)-2-methylbenzamide and 3,5-dichloro-N,N-dimethyl-2-hydroxybenzamide.</p>	◆	◆	
16	<p>Chemical structure of compound 16: 3,5-dichloro-N-(hydroxymethyl)benzamide.</p>	◆		
17 [60, 64]	<p>Chemical structure of compound 17: 3,5-dichloro-N-methyl-N-(carboxymethyl)benzamide and 3,5-dichloro-N-methyl-N-(formylmethyl)-2-hydroxybenzamide.</p>	◆		◆
18	<p>Chemical structure of compound 18: A complex bicyclic structure with a benzene ring fused to a seven-membered ring containing an amide and a carbonyl group.</p>	◆		

Table 4.7 shows representative of all intermediates appeared in LC/MS spectrum, which includes the structure of each unknown intermediates evaluated. Products were identified based on the molecular ion and mass spectrometric fragmentation peak. The results reveal that different pH of solution has different adsorption properties, which affect the reaction between diuron and the catalyst surface.

The addition of hydroxyl group onto the molecule, which supports the previous reports about the attack by hydroxyl radicals during the photocatalytic reaction, is also evidenced. The sites for hydroxyl radical to attack can be divided into two positions, i.e., the aromatic ring and the alkyl group. Although the detailed mechanisms of diuron degradation on zinc oxide and on titania are different, the main photocatalytic degradation pathways remained the same. They include hydroxylation of the aromatic ring and of the side chain (resulting in compound 4, 12, 15, and 17), dehalogenation or dechlorination of the aromatic ring (resulting in compound 1-5, 7, 10, and 13), demethylation (resulting in compound 12), and condensation (resulting in compound 14).

The sites for hydroxyl radical to attack can be divided into two regions, the aromatic ring and the alkyl group. When hydroxyl radical attacks the aromatic ring, it is more energetically favorable to attack carbon atom instead of chlorine atoms [42]. From the identified intermediates, a potential mechanism involving the reaction with the aromatic ring is shown as follows:

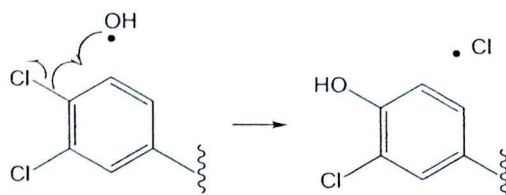


Figure 4.27 Dechlorination reaction.

Figure 4.27 can continue with the reaction with another hydroxyl radical and O_2 to add another hydroxyl group to the aromatic ring [67] as shown in Figure 4.28.

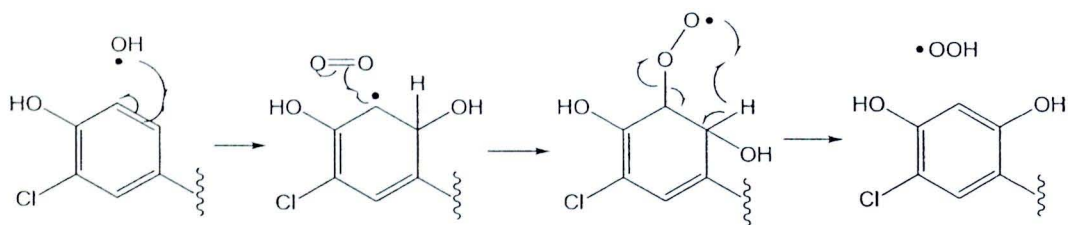


Figure 4.28 Hydroxylation reaction.

The attack of hydroxyl radical on the carbon of methyl group through hydrogen atom abstraction is energetically favorable [42]. The oxidation of methyl group yields an alcohol, and subsequently gets further oxidized to yield aldehyde and carboxylic acid, which then undergoes decarboxylation as shown in Figure 4.29.

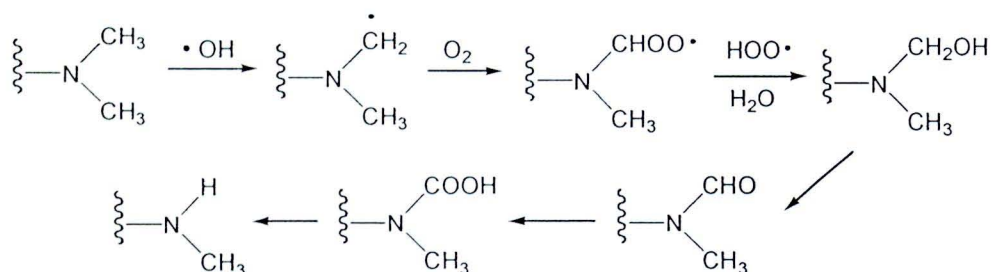


Figure 4.29 Decarboxylation reaction.

The analyzed of the first intermediate products suggest that substitution of chlorines and hydroxylation by hydroxyl radicals are the main degradation process of diuron before opening of the aromatic ring. Primary attack of diuron molecules by the hydroxyl radical is correlated with the frontier electron densities. So that primary position for hydroxyl radical attack are expected to be located on atoms with largest electron density [42].

4.4.1.2 Effect of UV Light

Photodegradation of diuron used zinc oxide as catalyst, for investigate the affect of UV-lamps to intermediate products. In this work, UV-lamps used were UV-A and UV-C. UV-A is a long wave (wave length ~ 360 nm), of which the energy is around $3.10 - 3.94$ eV per photon. UV-C is a short wave (wave length ~ 254 nm), of which the energy is $4.43 - 4.40$ eV per photon [68]. Both of UV-lamps were 1.5 Watt in power. In this process, the catalyst is activated by UV radiation. The photocatalysis can be defined as the acceleration of a photoreaction by the presence of a catalyst that can be activated by the absorption of light of energy greater than its band gap (3.2 eV for zinc oxide). From the research, it was found that the use of UV-A irradiation without catalyst, i.e. photolysis can degrade diuron by less than 5% even after 6 hours of irradiation. On the other hand, the photolysis by UV-C irradiation can degraded diuron up to 89% as shown in Figure 4.30. Thus intermediates generated from UV-C irradiation with catalyst might not be the effect from the catalyst.

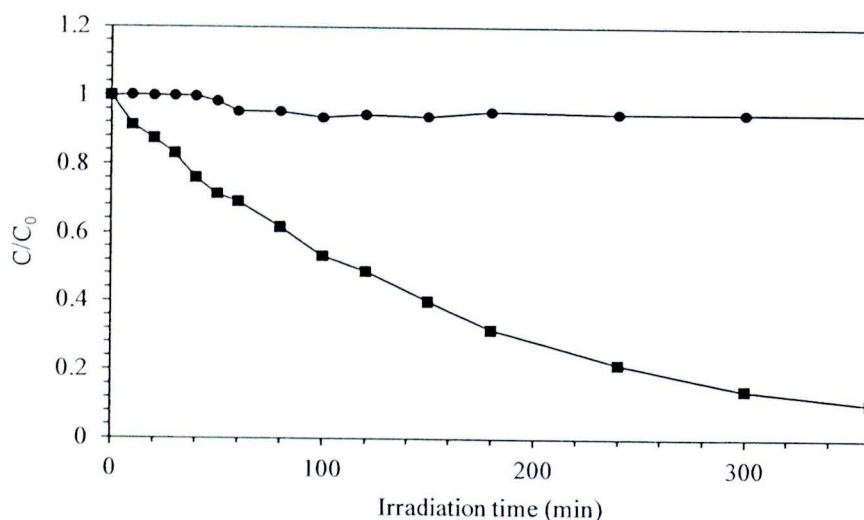


Figure 4.30 The effect of UV-lamp, i.e. (●) UV-A, (■) UV-C on the photolysis of diuron.

In Figure 4.31 shows the effect of UV-irradiation on degradation of diuron using zinc oxide as catalyst. The results reveal that diuron is degraded by 98% and 95% from the use of UV-A and UV-C respectively. The first orders plots are shown in Figure 4.32 and the apparent rate constant are shown in the Table 4.8. The reaction rate constant and the adsorption rate constant of diuron in the investigation of the effect of UV lamps based on the Langmuir-Hinshelwood model are shown in the Table 4.8.

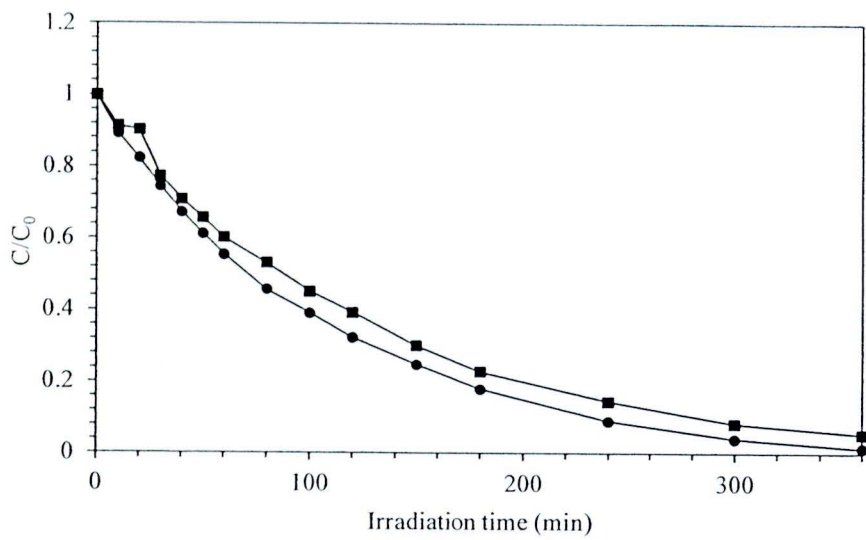


Figure 4.31 The effect of UV-lamp, i.e. (•) UV-A, (■) UV-C on the degradation of diuron using zinc oxide as catalyst.

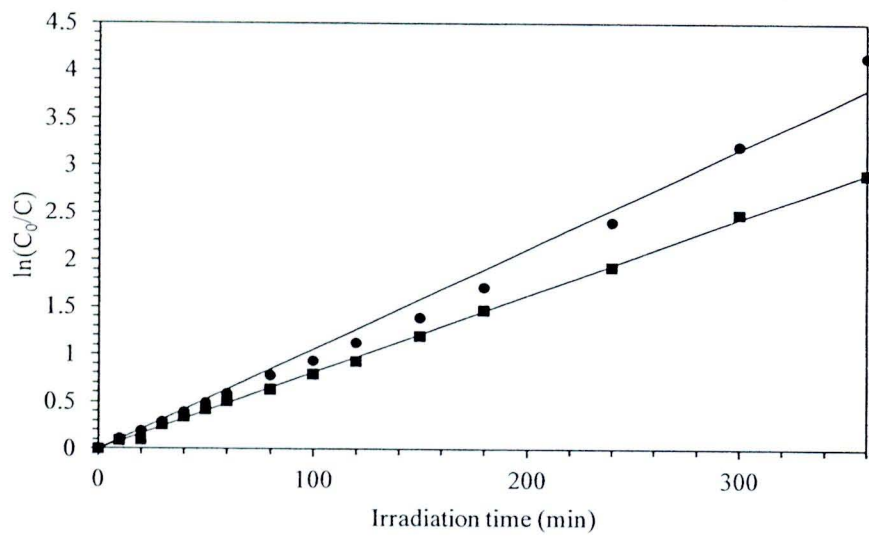


Figure 4.32 First order linear transforms of the photodegradation efficiency of diuron, (•) UV-A, (■) UV-C on the degradation of diuron using zinc oxide as catalyst.

Table 4.8 The apparent rate constant (k_{app}), reaction rate constants (k_r), and the adsorption constant (K) for the photocatalytic degradation of diuron using zinc oxide at different UV lamp.

Lamp	Pseudo first-order model		Langmuir-Hinshelwood model		
	$k_{app}(\text{min}^{-1})$	R^2	$k_r(\text{ppm}/\text{min})$	$K(\text{min}^{-1})$	R^2
UV-A	0.0106	0.9878	0.2073	0.0634	0.9968
UV-C	0.0081	0.9991	2.6165	0.0031	0.9991

The results show the photodegradation of diuron follows the pseudo first order kinetics and consistent with the Langmuir – Hinshelwood model.

Figure 4.33 and 4.34 shows the intermediates generated during photocatalytic degradation of diuron on zinc oxide using diferent UV-lamps. It was found that 10 intermediates were detected by HPLC when UV-A lamps were used while the use of UV-C yielded only 3 kinds of intermediates.

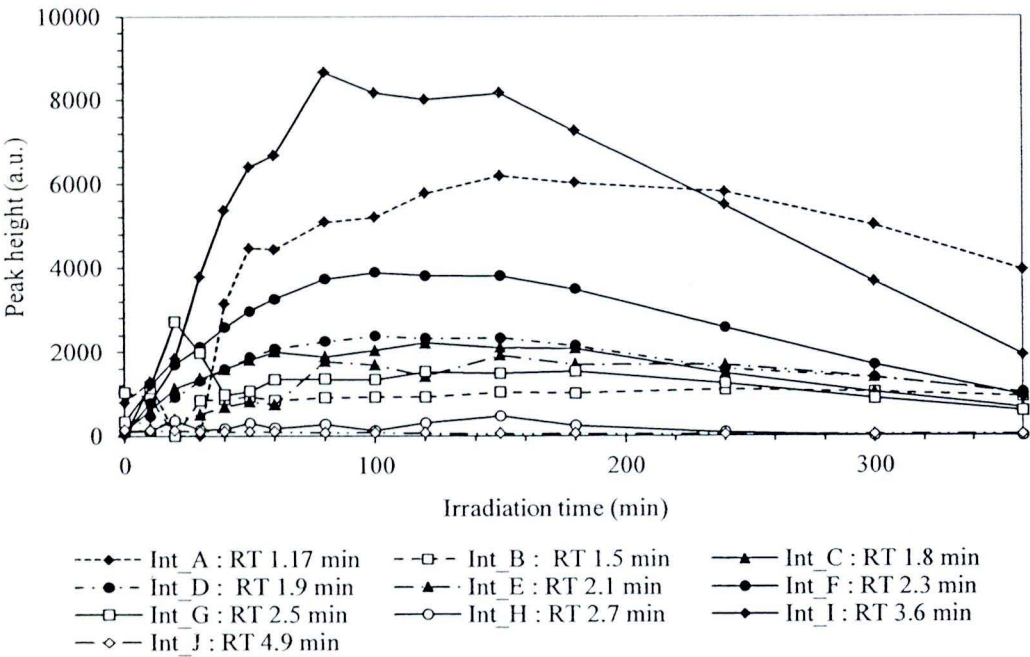


Figure 4.33 HPLC peak height of intermediates generated during photocatalytic degradation on diuron on zinc oxide using UV-A as light source.

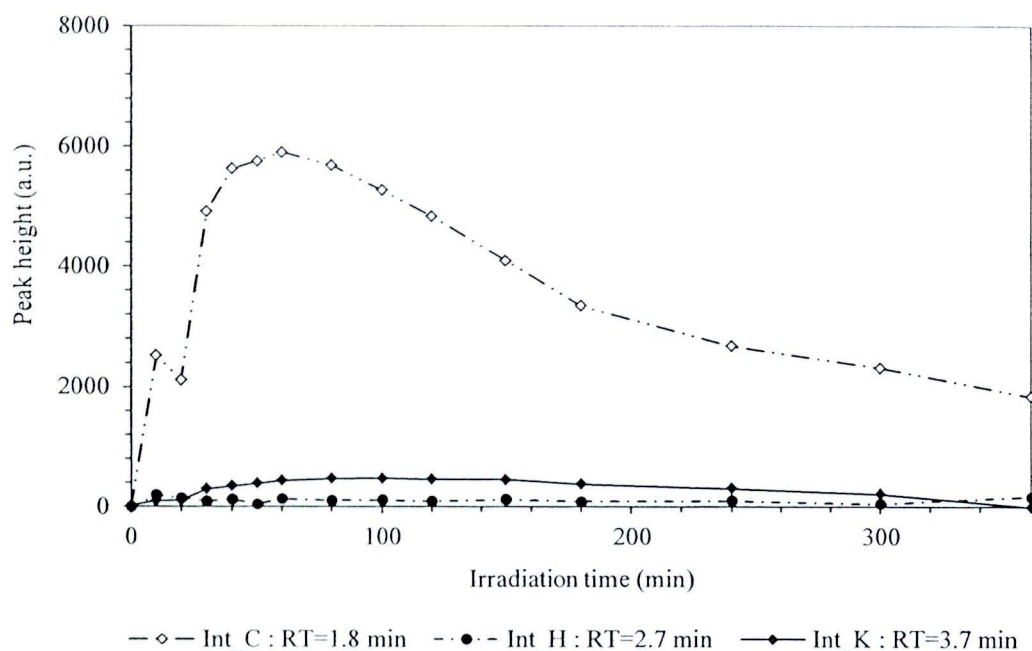


Figure 4.34 HPLC peak height of intermediates generated during photocatalytic degradation on diuron on zinc oxide using UV-C as light source.

It was found that the concentration of the intermediates also changes along the course of the photodegradation. The intermediates are generated and consumed within the short time. The UV-light affects the generation of intermediates. The use of UV-A, most intermediates are formed after 60 minutes of the irradiation time whereas the intermediates from UV-C are generated after 30 minutes. The structures of the intermediates product were identified by LC-MS as shown in Table 4.9. It was found that the result is contrary with HPLC analysis for the intermediates generates from UV-C. It can be suggested that each unknown intermediates are presented at very low concentration. However these small molecules are not detectable by HPLC analysis.

Table 4.9 Possible intermediates generated from photodegradation of diuron on zinc oxide using different kind of UV-lamp.

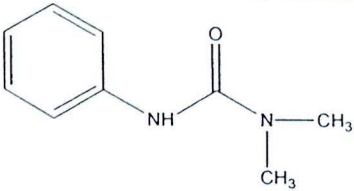
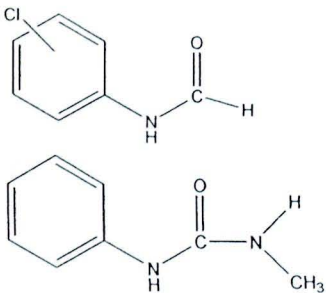
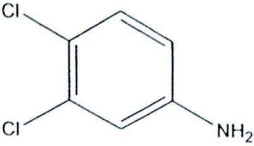
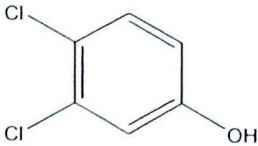
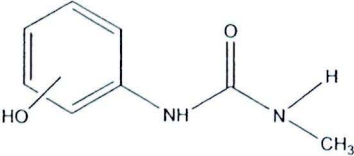
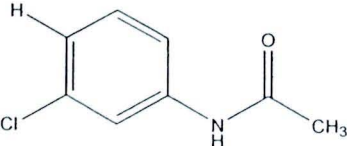
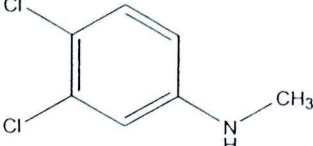
Compound	Propose structure	UV-A	UV-C
1 [60]			◆
2 [61]		◆	
3 [1, 60, 61, 65]		◆	
4		◆	
5 [44]			◆
6		◆	◆
7			◆

Table 4.9 (continued)

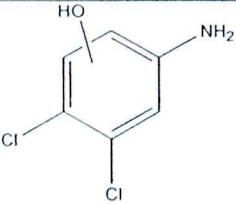
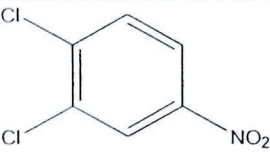
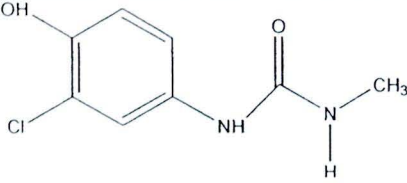
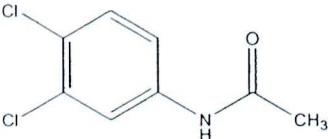
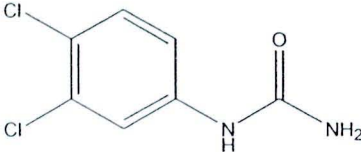
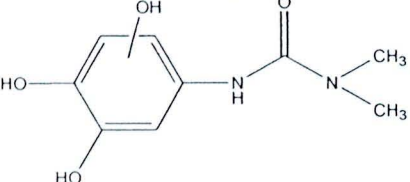
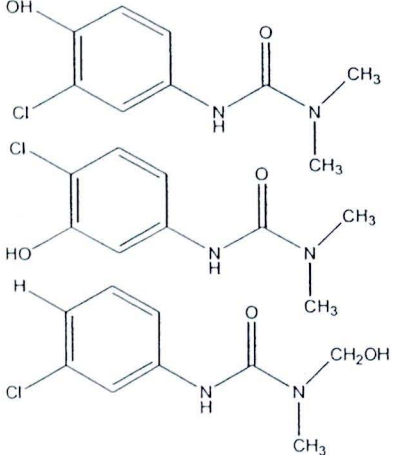
Compound	Propose structure	UV-A	UV-C
8 [62]			◆
9 [69]		◆	
10 [62]			◆
11		◆	◆
12 [70]		◆	◆
13 [66]			◆
14 [1, 60, 64]		◆	

Table 4.9 (continued).

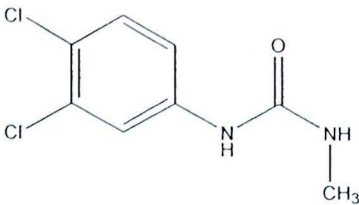
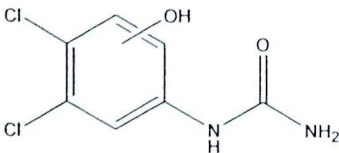
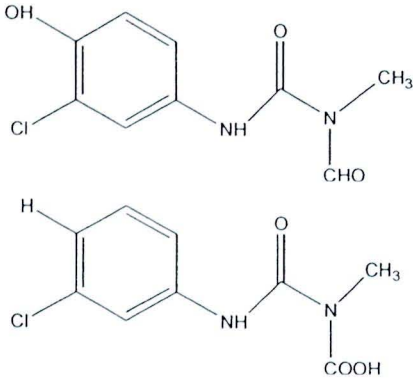
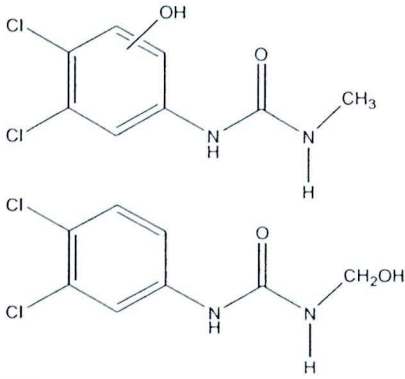
Compound	Proposed structure	UV-A	UV-C
15 [42, 61, 64]		◆	◆
16		◆	
17			◆
18 [70]		◆	

Table 4.9 (continued).

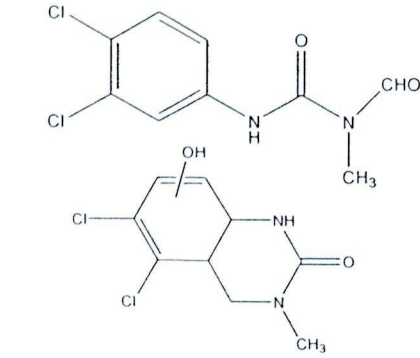
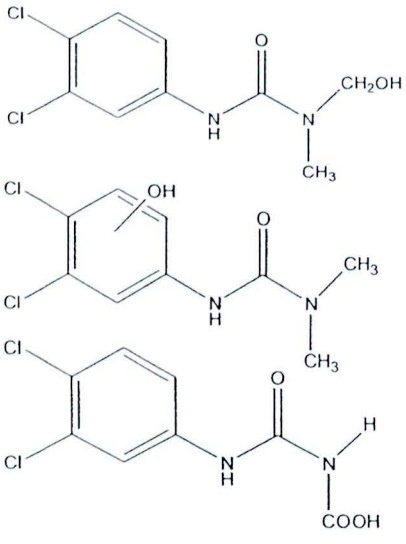
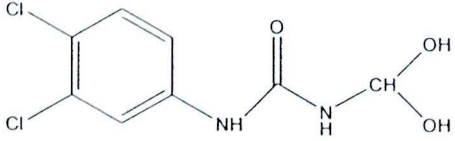
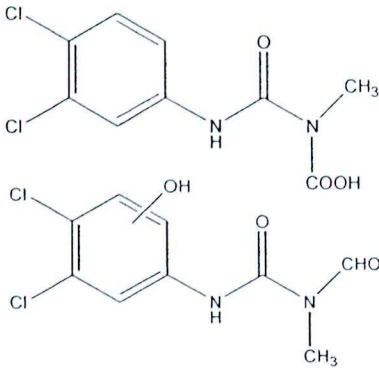
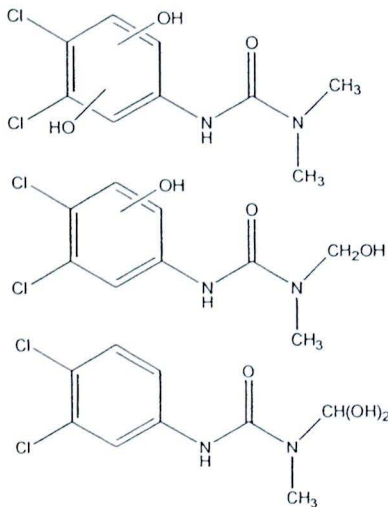
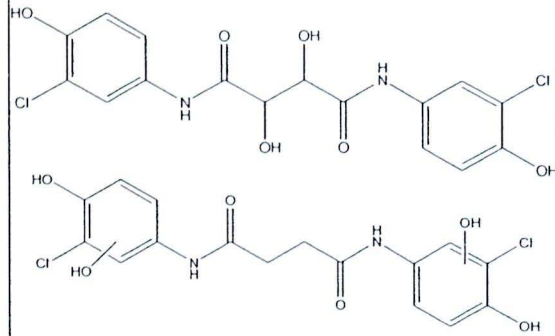
Compound	Proposed structure	UV-A	UV-C
19 [60, 62, 64, 65]		◆	◆
20 [60, 64, 65]		◆	◆
21			◆

Table 4.9 (continued).

Compound	Proposed structure	UV-A	UV-C
22 [42, 60]		◆	◆
23 [42, 62]		◆	
24		◆	

Several transformation products were detected. They correspond to the following reactions: the hydroxylation occurring on the aromatic ring (compounds 5, 8, 13, 16, 18, and 20), dechlorination (compounds 1, 2, 6, 10, 14, and 17), demethylation (compounds 2, 5, 10, 12, 15, and 19) and condensation (compound 19).

Diuron is degraded into smaller compounds during photodegradation process. At the same time, these radicals generated during photodegradation can form conjugates and resulted in a larger molecule. Larger molecules were observed in this experiment. For larger molecules, more complex combination of radicals and rearrangement can occur. More information is needed to determine the structure.

4.4.2 Photodegradation on titanium dioxide

4.4.2.1 Effect of pH of diuron solution

When titanium dioxide was employed as the catalyst, intermediates were also detected by HPLC during the photocatalytic treatment. Figure 4.35-4.36 and Table 4.9 shows the extent of photodegradation of diuron at pH 3, 7, and 10. The results for the degradation are illustrated in Figure 4.35. The first order transform plots are giving in Figure 4.36 whereas the apparent rate constants are shown in Table 4.9. The data shown in Figure 4.35 were fitted against the Langmuir-Hinshelwood kinetic model. The results are shown in Table 4.10, including the apparent rate constant, calculated reaction rate constants and the calculated adsorption constant based on the Langmuir-Hinshelwood kinetic model, of photodegradation of diuron at various pH.

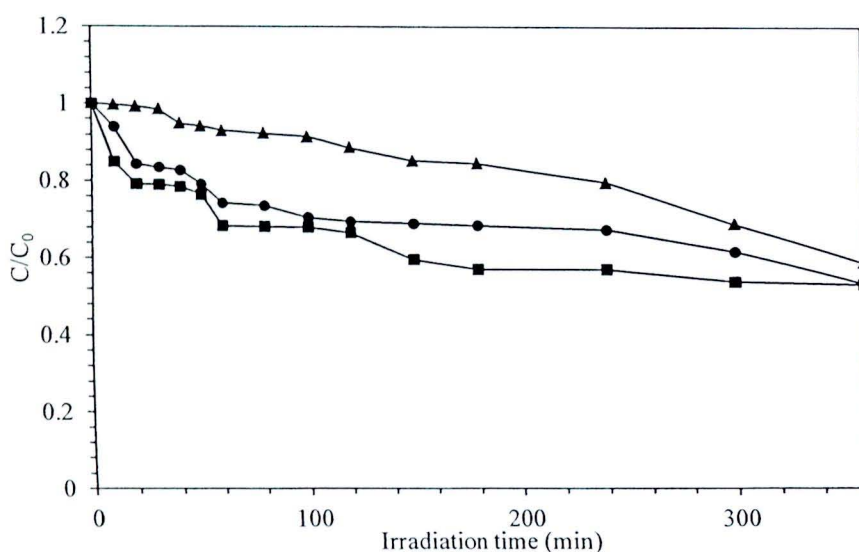


Figure 4.35 Effect of pH of the solution on photodegradation efficiency of diuron on titania. The pH is adjusted at pH 3 (■), pH 7 (●), and pH 10 (▲).

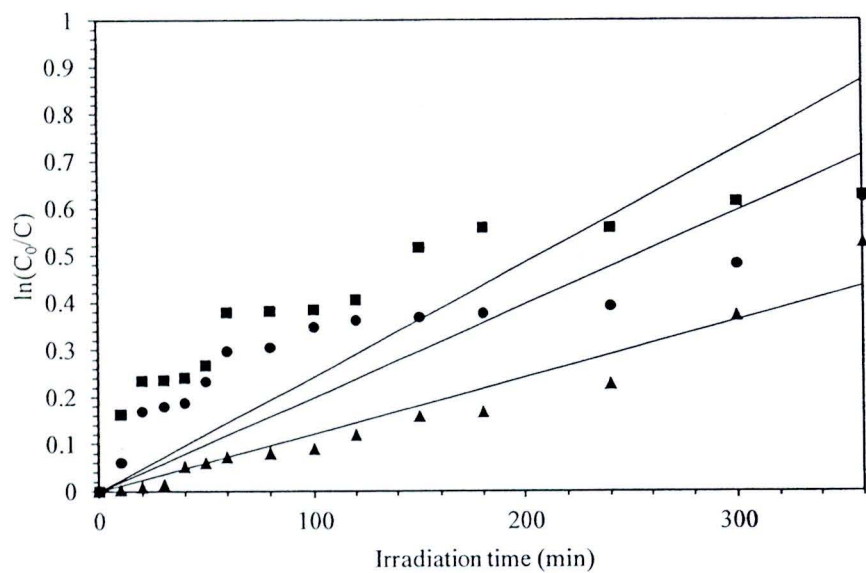


Figure 4.36 First order linear transforms of the photodegradation efficiency of diuron on titania at various pH values. The pH is adjusted at pH 3 (■), pH 7 (●), and pH 10 (▲).

Table 4.10 The apparent rate constant (k_{app}), reaction rate constants (k_r), and the adsorption constant (K) for the photocatalytic degradation of diuron using zinc oxide at at various pH of solution.

pH of solution	Pseudo first-order model		Langmuir-Hinshelwood model		
	$k_{app}(\text{min}^{-1})$	R^2	$k_r(\text{ppm}/\text{min})$	$K(\text{min}^{-1})$	R^2
3	0.0024	0.8584	0.9993	0.2450	0.7069
7	0.0020	0.8856	2.4618	0.0008	0.8969
10	0.0012	0.9672	0.9512	0.6677	0.8404

The results indicate that the photodegradation is increased with decreasing pH down to pH 3. At pH 3, 7, and 10, it was found that diuron was degraded by about 46, 46, and 41%, respectively. It can be seen that the pH has a weak effect on the degradation of diuron. However an acidic condition seems to accelerate the degradation kinetics of diuron in the

aqueous solution. Since the reaction mainly occurs at surface of the catalyst therefore, the pH effect should be explained by differences on adsorption with pH [71]. It has been reported that the point of zero charge for titanium dioxide is about 5.6-5.8 [72]. In neutral solution, the surface charge is neutral, whereas at pH lower than 5.6, the surface charge is positive. As a consequence, in acidic solution, molecules are attracted to the surface by their electronegative part [71]. For pH higher than the point zero charge, the surface becomes negative charged. At $\text{pH} < \text{pH}_{\text{pzc}}$ the surface is positive charged according to the following equilibrium:



When titanium dioxide was employed as the catalyst and the solution was adjusted to different pH, various kinds of intermediates were detected by HPLC during the photocatalytic treatment. The results are shown in Figure 4.37-4.39. There are 12, 13, and 16 kinds of intermediates formed from the reaction at pH 3, 7, and 10, respectively. Although quantitative data were not obtained, concentrations of these intermediates are expected to be very low, since the intensities of the HPLC signals for the intermediates are much lower than that of diuron. The concentration of the intermediates also change along the course of the photodegradation.

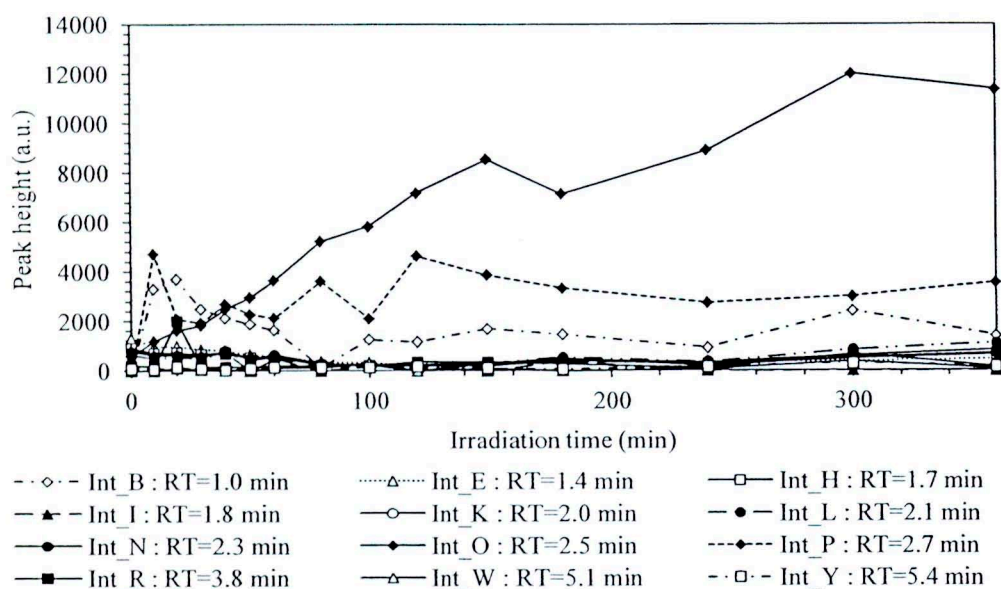


Figure 4.37 HPLC peak height of intermediates generated during photocatalytic degradation on diuron on titanium dioxide and the initial pH of solution 3.

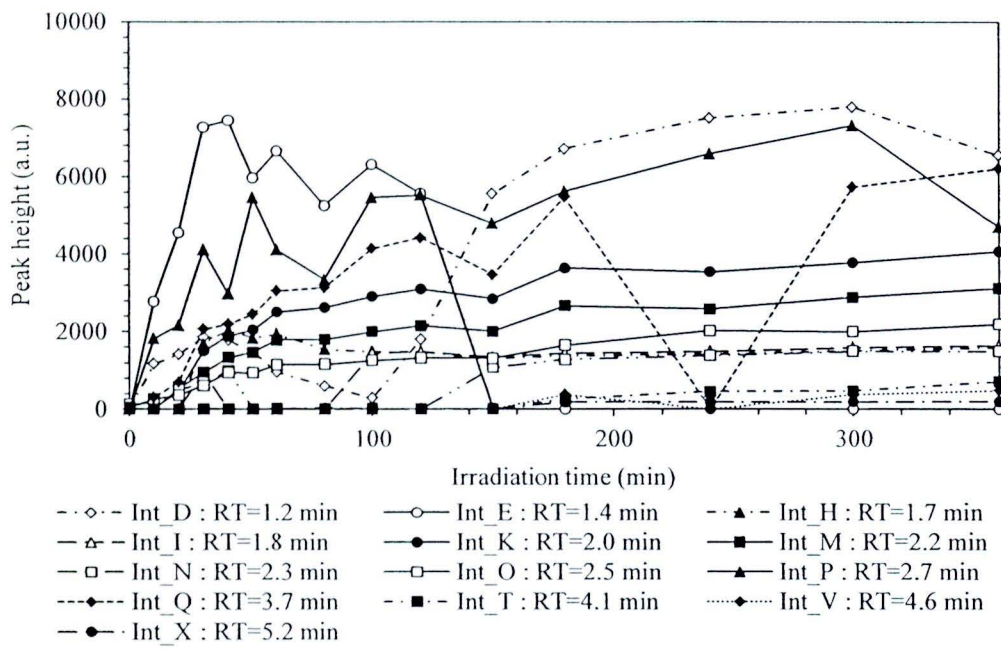


Figure 4.38 HPLC peak height of intermediates generated during photocatalytic degradation on diuron on titanium dioxide and the initial pH of solution 7.

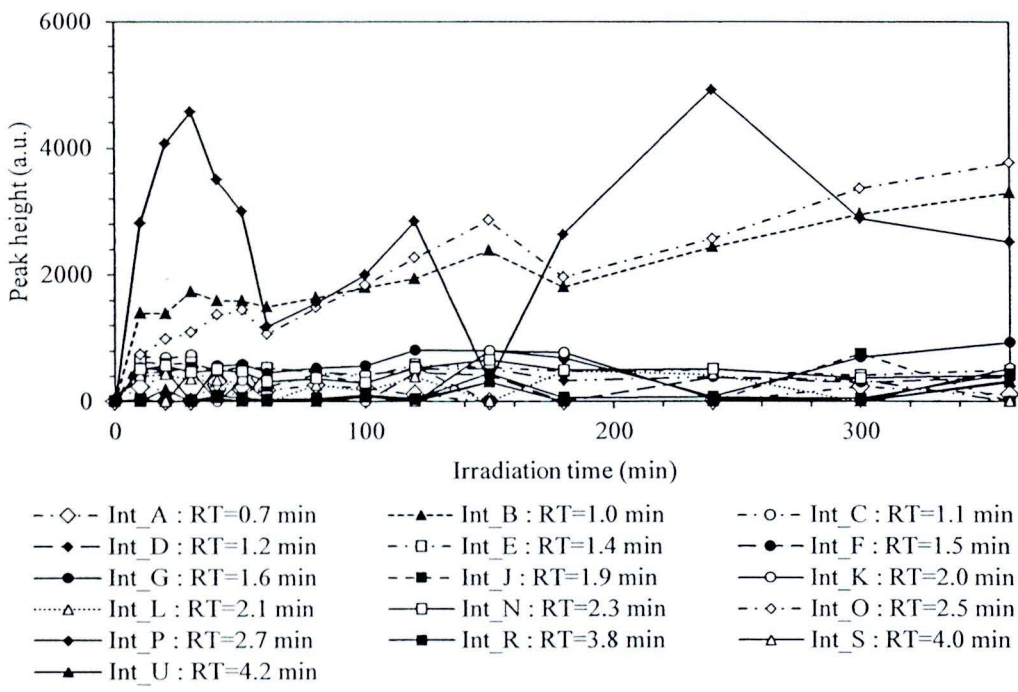


Figure 4.39 HPLC peak height of intermediates generated during photocatalytic degradation on diuron on titanium dioxide and the initial pH of solution 10.

The intermediate products are presented at very low concentration, the data show some fluctuation. Concentration of intermediate increase with irradiation time, and intermediate can be disappear even after 6 hours, some intermediate remain stable even after 6 hours of the reaction.

Comparison of the intermediates formed from the reaction at various pH of solution, reveals common intermediates as well as different intermediates. The attempts were made to identify the intermediate products through analysis using LC-MS. The structures of all intermediates detected are proposed in Table 4.11.

Results obtained when titanium dioxide is used as photocatalyst show that the distribution of products depends on the pH of the solution. In neutral solution, the attack of the hydroxyl radicals is located both on the aromatic ring and on the methyl groups. In acidic solution, it is mainly located on the methyl groups [71].

Table 4.11 Possible intermediates generated from photodegradation of diuron on titanium dioxide at pH of 3, 7, and 10.

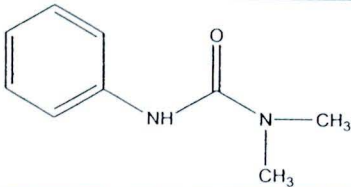
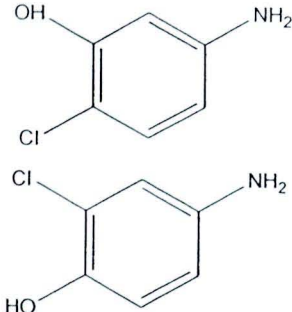
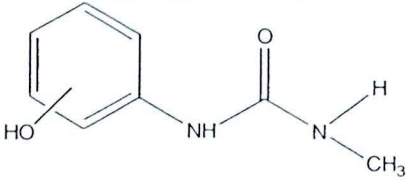
Compound	Structure	pH3	pH7	pH10
1 [60]		◆		
2		◆		◆
3 [44]		◆	◆	◆

Table 4.11 (continued).

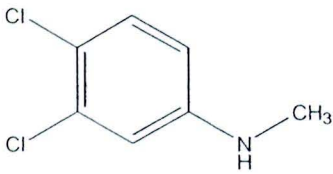
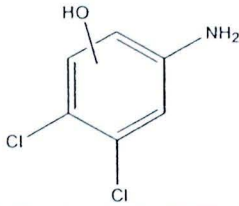
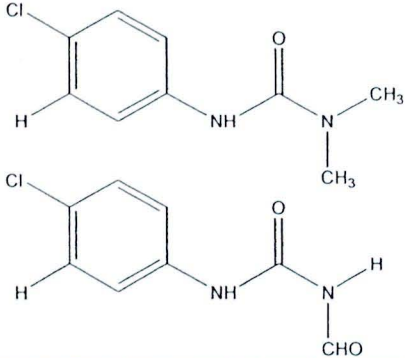
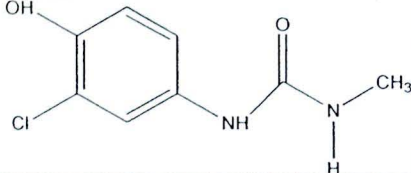
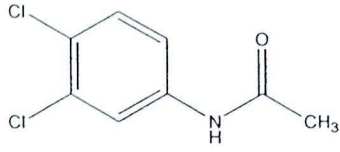
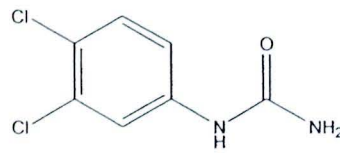
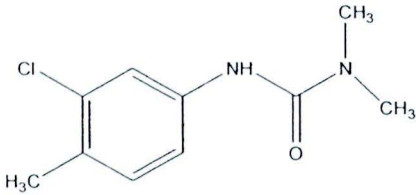
Compound	Structure	pH3	pH7	pH10
4		◆		
5 [62]		◆		
6		◆		
7 [62]		◆	◆	◆
8		◆	◆	
9 [70]		◆		
10 [63]				◆

Table 4.11 (continued).

Compound	Structure	pH3	pH7	pH10
11 [66]		◆	◆	
12 [42, 61, 64]		◆	◆	◆
13		◆		◆
14		◆	◆	◆
15.1 [60, 62, 64, 65]		◆	◆	

Table 4.11 (continued).

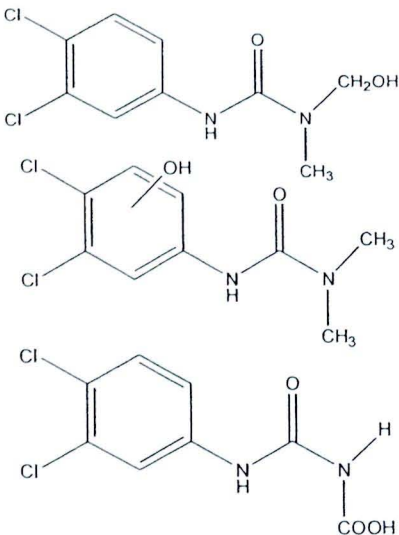
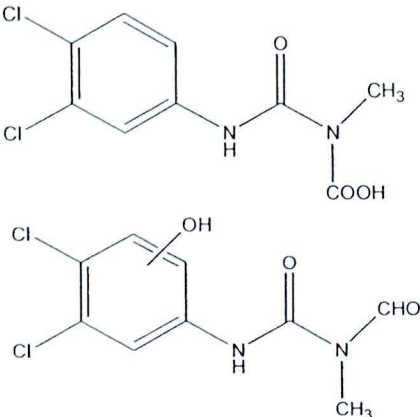
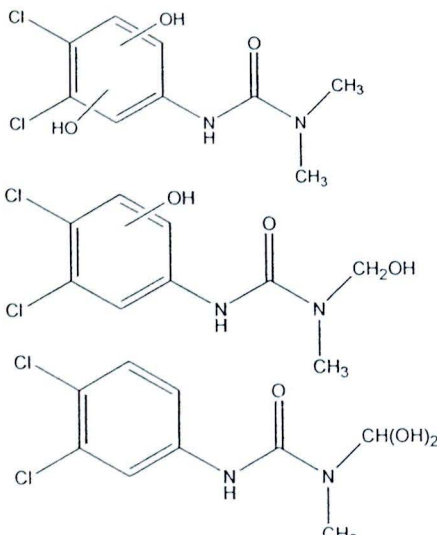
Compound	Structure	pH3	pH7	pH10
16 [60, 64, 65]			◆	
17 [60, 64]		◆		
18 [42, 62]		◆		

Table 4.11 (continued).

Compound	Structure	pH3	pH7	pH10
19		◆		◆

Different pH of solution has different adsorption properties, which affect the reaction between diuron and the catalyst surface. The possible degradation pathway is proposed in these steps, first, the attack on the aromatic ring by OH^\cdot radical without dechlorination or alkyl chains. The next step involved a series of oxidation process that eliminated alkyl groups and chlorine atom. The last step involved the oxidative opening of aromatic ring, leading to small organic ion and inorganic species.

4.4.2.2 Effect of UV light

Figure 4.40 shows the photocatalytic degradation of diuron using titanium dioxide as catalyst and the UV irradiation, source is either UV-A or UV-C. The results indicate that photodegradation of diuron by UV-C irradiation can reach 90% within 6 h, while the use of UV-A results in only 45% degradation. However, high degradation rate achieved with UV-C is partly due to photolysis of diuron by UV-C. The first orders plots are shown in Figure 4.41 and the apparent rate constant are shown in the Table 4.12. The reaction rate constant and the adsorption rate constant of diuron in the investigation of the effect of UV lamps based on the Langmuir-Hinshelwood model are shown in the Table 4.12.

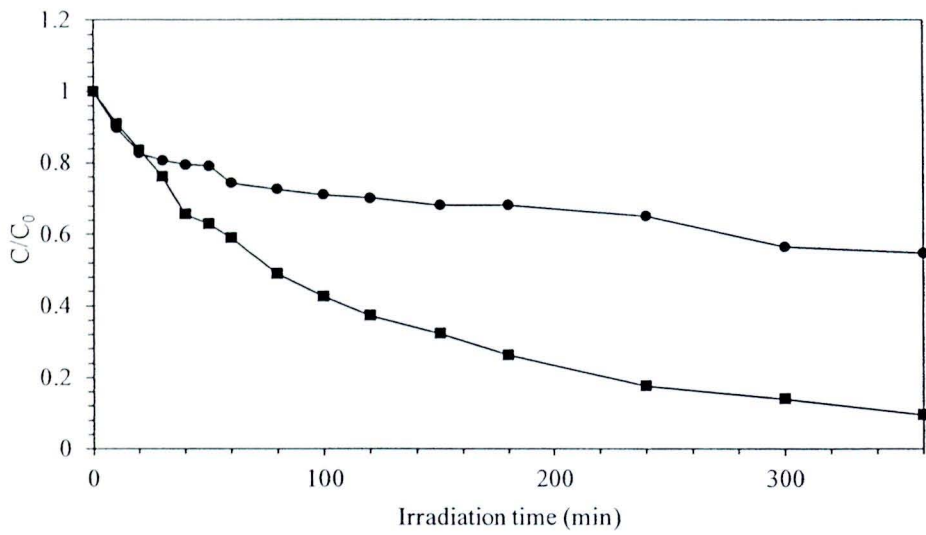


Figure 4.40 The effect of UV-lamp (●) UV-A, (■) UV-C on the degradation of diuron using titania as catalyst.

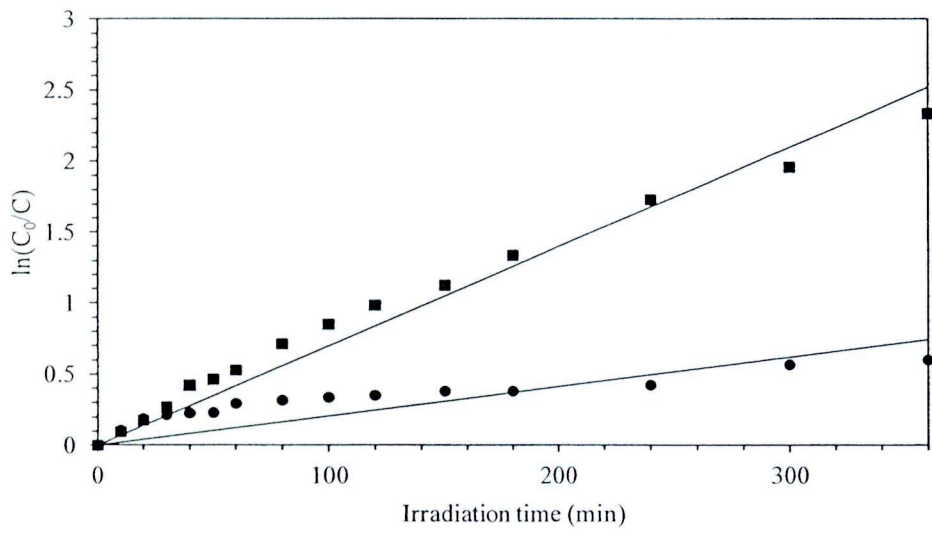


Figure 4.41 First order linear transforms of the photodegradation efficiency of diuron, (●) UV-A, (■) UV-C on the degradation of diuron using titania as catalyst.

Table 4.12 The apparent rate constant (k_{app}), reaction rate constants (k_r), and the adsorption constant (K) for the photocatalytic degradation of diuron using titania at different UV lamp.

Lamp	Pseudo first-order model		Langmuir-Hinshelwood model		
	$k_{app}(\text{min}^{-1})$	R^2	$k_r(\text{ppm/min})$	$K(\text{min}^{-1})$	R^2
UV-A	0.0021	0.8847	0.0025	0.1218	0.9979
UV-C	0.0041	0.9579	0.9988	0.0952	0.8866

The results show that the photodegradation of diuron on titania is inconsistent with the Langmuir – Hinshelwood model for both cases, i.e. UV-A and UV-C because KC is close to 1.

Figure 4.42 and 4.43 shows the profile of intermediates generated during photocatalytic degradation of diuron on titanium dioxide using different UV-lamps. It was found that 11 and 9 kinds of intermediates are formed when UV-A and UV-C was used, respectively. The intermediates were detected by HPLC and identified the intermediates by LC-MS as shown in the Table 4.13.



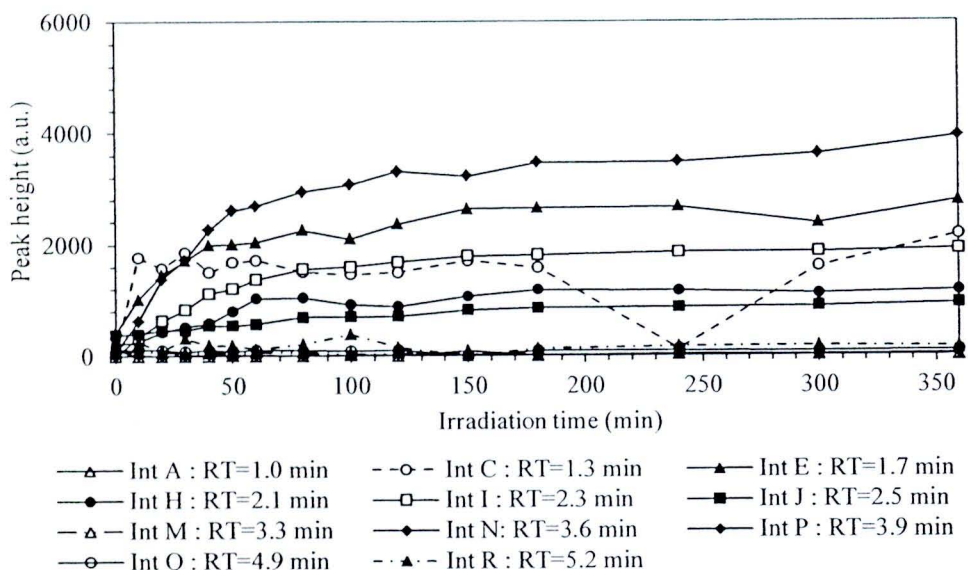


Figure 4.42 HPLC peak height of intermediates generated during photocatalytic degradation on diuron on titanium dioxide using UV-A as light source.

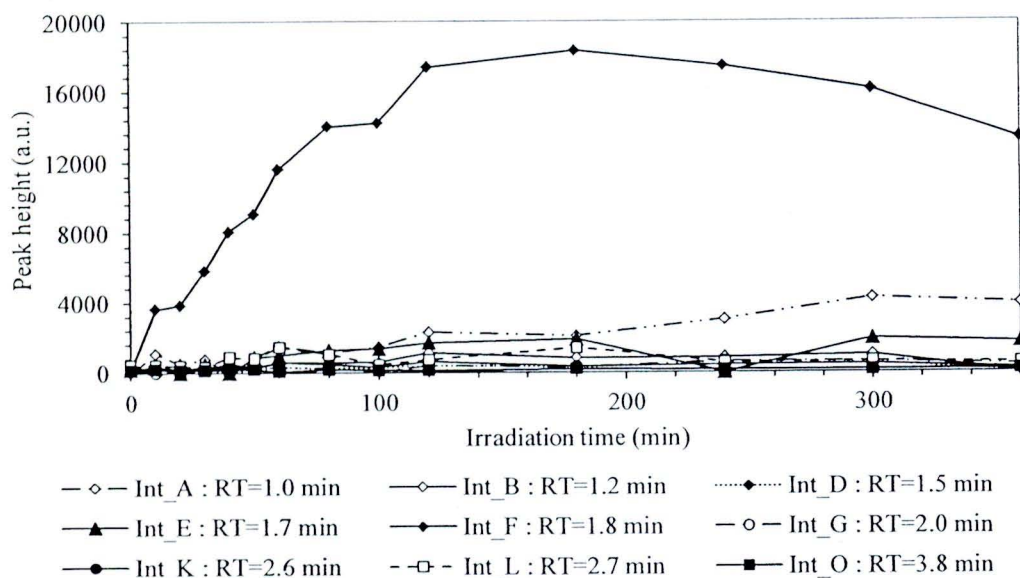


Figure 4.43 HPLC peak height of intermediates generated during photocatalytic degradation on diuron on titanium dioxide using UV-C as light source.

The intermediates are produced and degraded fast during the reaction and some intermediates remain stable even after 6 hours of the reaction. It was found that the concentration of the intermediates also changes along the course of the photodegradation. The structures of the intermediates product were identified by LC-MS as shown in Table 4.13.

Table 4.13 Possible intermediates generated from photodegradation of diuron on titanium dioxide using different UV-lamp.

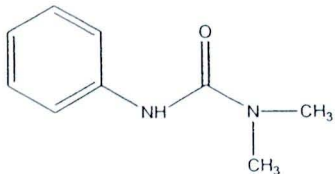
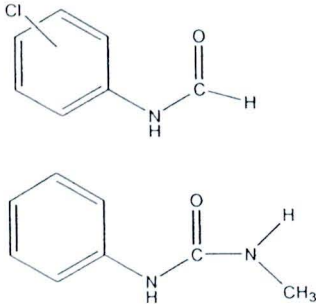
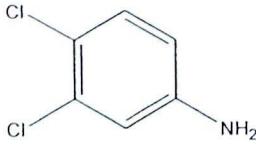
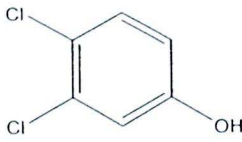
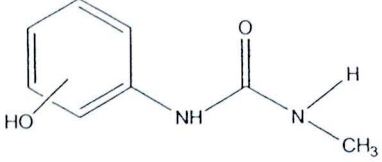
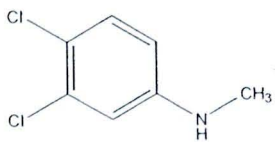
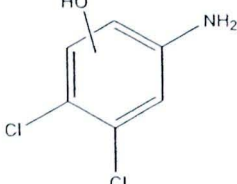
Compound	Proposed structure	UV-A	UV-C
1 [60]			◆
2 [61]		◆	
3 [1, 60, 61, 65]		◆	
4		◆	
5 [44]			◆
6		◆	◆
7 [62]		◆	◆

Table 4.13 (continued).

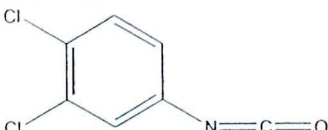
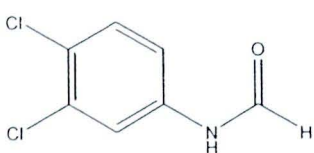
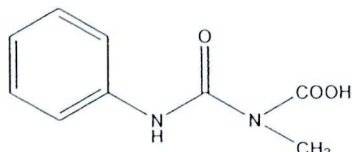
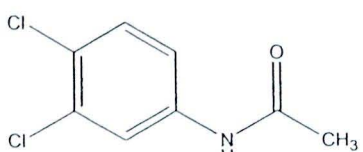
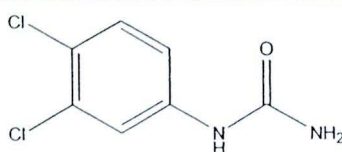
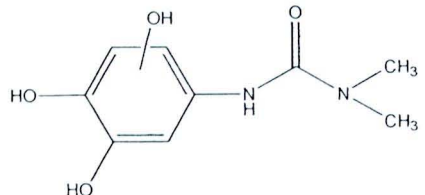
Compound	Proposed structure	UV-A	UV-C
8 [69]		◆	
9 [64]		◆	
10 [66]		◆	
11		◆	
12 [70]		◆	
13 [66]		◆	

Table 4.13 (continued).

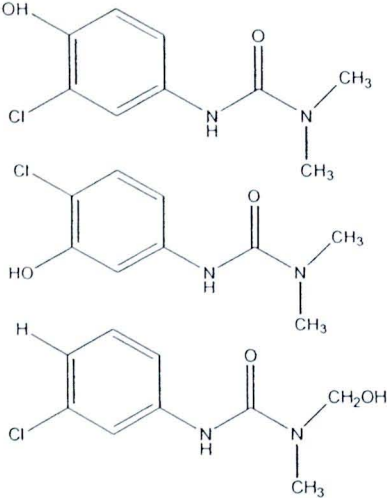
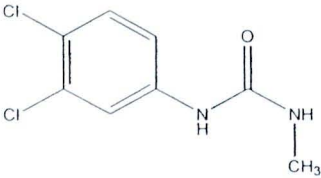
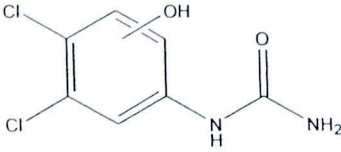
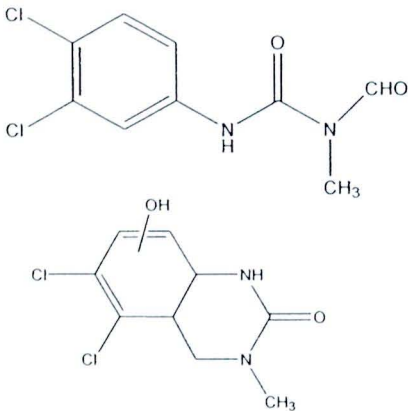
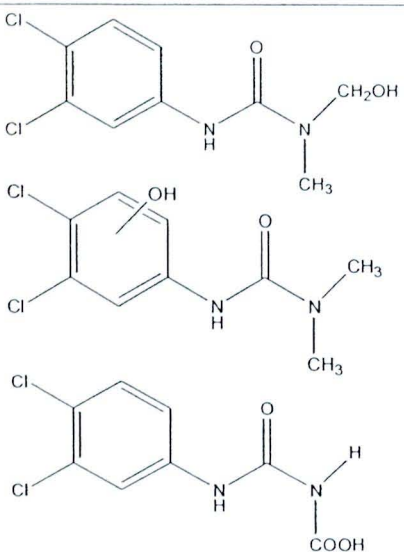
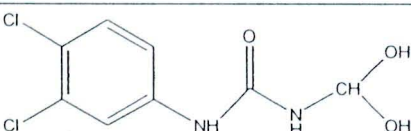
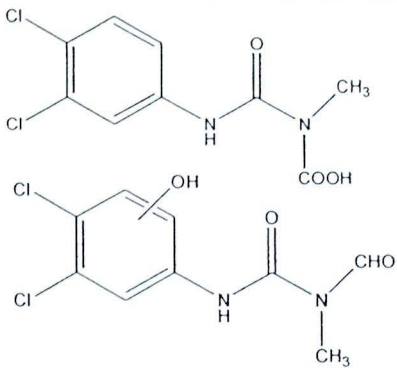
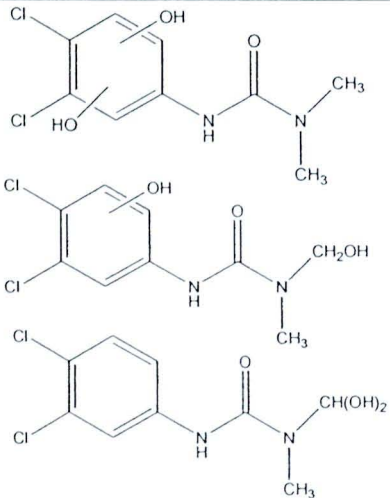
Compound	Proposed structure	UV-A	UV-C
14 [1, 60, 64]		◆	◆
15 [42, 61, 64]		◆	◆
16		◆	◆
17 [60, 62, 64, 65]		◆	◆

Table 4.13 (continued).

Compound	Proposed structure	UV-A	UV-C
18 [60, 64, 65]		◆	
19			◆
20 [60, 64]			◆
21 [42, 62]			◆

UV-light also affects the generation of intermediates Diuron is degraded into smaller compounds during photodegradation process. The degradation rate when using UV-C on titania was faster than using UV-A, the formation of intermediates when using UV-C was also rapid. The possible degradation mechanism of diuron on titania is proposed in Table 4.13 are similar to the mechanism of diuron on zinc oxide.

4.4.3 Effect of type of photocatalysts

Comparison of the intermediates formed from the reaction using different photocatalysts, i.e., titanium dioxide and zinc oxide, reveals common intermediates as well as different intermediates. Attempts were made to identify the intermediate products through analysis using LC-MS. The results confirm that the degradation of diuron generates lots of intermediates. According to the detailed analysis of the obtained mass spectrum, it indicates that the peak detected by HPLC chromatogram (i.e., an intermediate presented in Figure 4.30 and 4.39) is indeed a signal from a collection of intermediates. The structures of all intermediates detected are proposed in Table 4.14. The molecular mass of each product was confirmed by its detection in negative or/and positive mode. The results confirm that diuron is degraded into smaller compounds during photodegradation. While some intermediates are further degraded by the photocatalytic process, the conjugation of intermediates to form larger molecules is also observed.

Table 4.14 Possible intermediates generated from photodegradation of diuron on zinc oxide and titania.

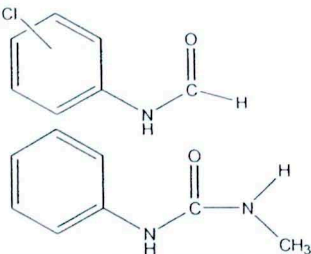
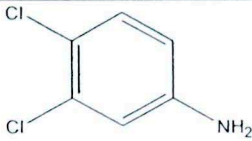
Compound	Proposed structure	ZnO	TiO ₂
1 [42]		◆	◆
2 [1, 60, 61, 65]		◆	◆

Table 4.14 (continued).

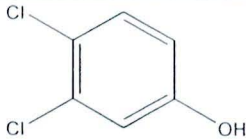
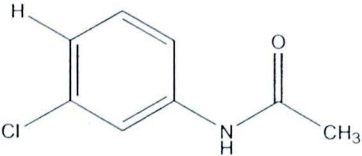
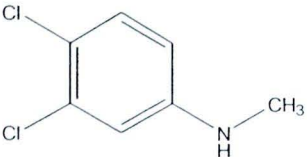
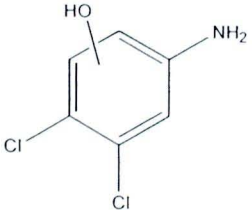
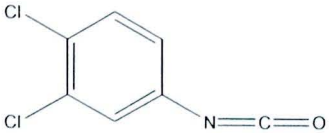
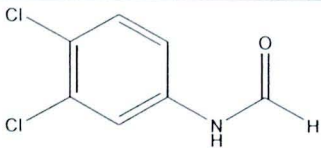
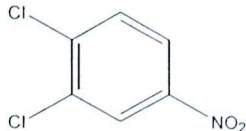
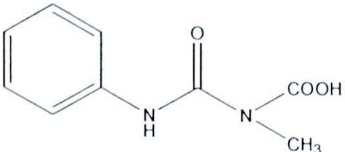
Compound	Proposed structure	ZnO	TiO ₂
3		◆	◆
4		◆	
5			◆
6 [62]			◆
7 [69]			◆
8 [64]			◆
9 [69]		◆	
10 [66]			◆

Table 4.14 (continued).

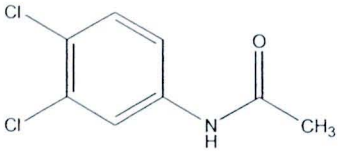
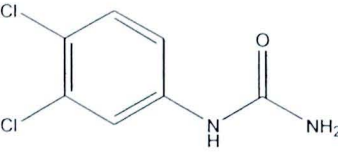
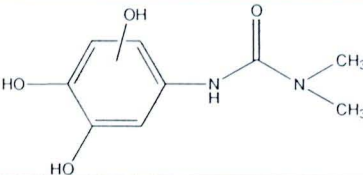
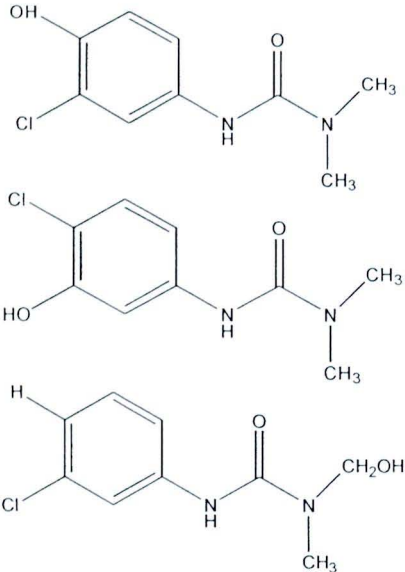
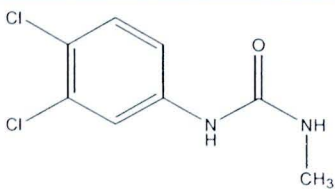
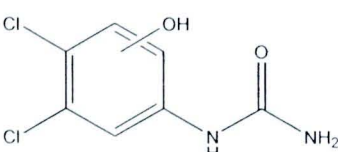
Compound	Proposed structure	ZnO	TiO ₂
11		◆	◆
12 [70]		◆	◆
13 [66]			◆
14 [1, 60, 64]		◆	◆
15 [42, 61, 64]		◆	◆
16		◆	◆

Table 4.14 (continued).

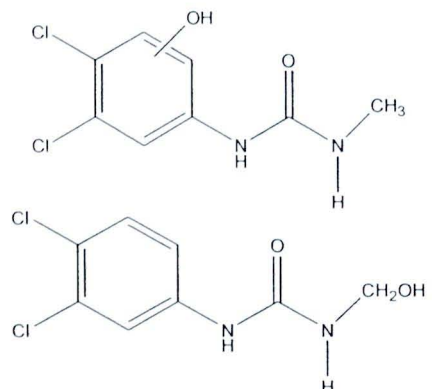
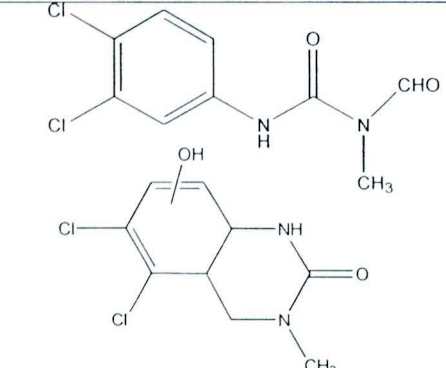
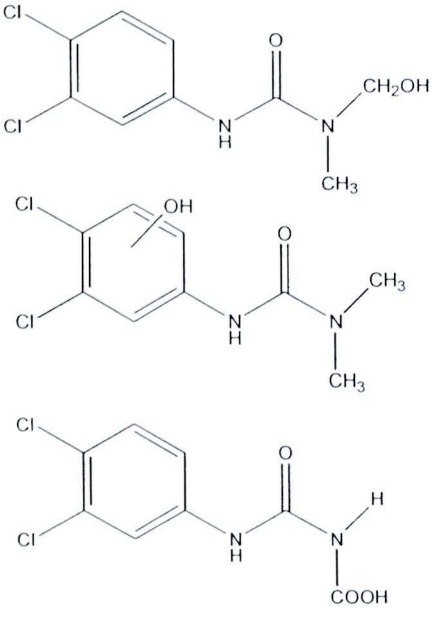
Compound	Proposed structure	ZnO	TiO ₂
17 [70]		◆	
18 [60, 62, 64, 65]		◆	◆
19 [60, 64, 65]		◆	◆

Table 4.14 (continued).

Compound	Proposed structure	ZnO	TiO ₂
20 [60, 64]		◆	
21 [42, 62]		◆	
22		◆	

Different type of catalyst has different surface properties, which affect the interaction between diuron and the catalyst surface. The dissimilarity in the degradation mechanism arises from the difference in interaction between the catalyst surface and the adsorbed diuron. As many of the intermediates listed in the Table 4.7, 4.9, 4.11, and 4.13 are common with those reported in other researches, it confirms that the main degradation pathway of diuron using zinc oxide and titanium dioxide follows the mechanisms previously proposed. They included hydroxylation of the aromatic ring and of the side chain (resulting in compounds 17, 19, 20, and 21), dehalogenation or dechlorination of the aromatic ring (resulting in compounds 1, 4, 14, and 22), demethylation (resulting in compound 12), and condensation (resulting in compound 18).

According to the detailed mass spectra shown in Appendix C, some intermediates product identified from LC-MS were analyzed by LC-MS/MS (MS/MS detector, mass spectrometric detector) which can confirm the structure of the intermediates. In this study, the investigation of intermediates was inconclusive as shown in Appendix D. It can be the result from the fact that the concentration of all unknown intermediates are very low. Therefore, signals from unknown intermediates are very low and does not explicit.